

DiskANN++: Efficient Page-based Search over Isomorphic Mapped Graph Index using Query-sensitivity Entry Vertex

Jiongkang Ni¹, Xiaoliang Xu¹, Yuxiang Wang¹, Can Li¹, Jiajie Yao², Shihai Xiao², Xuecang Zhang²

¹ Hangzhou Dianzi University, Hangzhou, China, ² Huawei Technologies Co., Ltd, Hangzhou, China
{hananoyuuki,xxl,lsswyx,lic}@hdu.edu.cn, {yaojiajie1,xiaoshihai,zhangxuecang}@huawei.com

Abstract—Given a vector dataset \mathcal{X} and a query vector \vec{x}_q , graph-based Approximate Nearest Neighbor Search (ANNS) aims to build a graph index G and approximately return vectors with minimum distances to \vec{x}_q by searching over G . The main drawback of graph-based ANNS is that a graph index would be too large to fit into the memory especially for large-scale \mathcal{X} . To solve this, a Product Quantization (PQ)-based hybrid method called DiskANN is proposed to store a low-dimensional PQ index in memory and retain a graph index in SSD, to reduce memory overhead while ensuring a high search accuracy. However, it suffers from two I/O issues that significantly affect the overall efficiency: (1) long routing path from the entry vertex to the query’s neighborhood and (2) redundant I/O requests during the routing process. We propose an optimized DiskANN++ to overcome above issues. Specifically, for the first issue, we present a *query-sensitive entry vertex selection strategy* to replace DiskANN’s static graph-central entry vertex by a dynamically determined entry vertex that is close to the query. For the second I/O issue, we present an *isomorphic mapping on DiskANN’s graph index to optimize the SSD layout* and propose an *asynchronously optimized Pagesearch based on the optimized SSD layout* as an alternative to DiskANN’s Beamsearch. Comprehensive experimental studies on real-world datasets demonstrate our DiskANN++’s superiority on efficiency, e.g., we achieve a notable 1.5 X to 2.2 X improvement on QPS compared to DiskANN, given the same accuracy constraint.

I. INTRODUCTION

Approximate Nearest Neighbor Search (ANNS) [1], [2] has been widely studied recently, which is fundamental for many real-world applications, such as recommendation systems [3], [4], information retrieval [5], [6], data mining [7], [8], and pattern recognition [9], [10]. Given a vector dataset \mathcal{X} and a query vector $\vec{x}_q \in \mathcal{X}$, ANNS aims to return approximate nearest neighbors to \vec{x}_q from \mathcal{X} with minimum distance [11]. ANNS is generally categorized as four types: *hashing-based* [12], [13], *tree-based* [14], [15], *quantization-based* [16], [17], and *graph-based* [18], [19] methods. Among them, graph-based ANNS attracts more attention and has been regarded as the most promising one due to its impressive efficiency and effectiveness over large-scale datasets [11], [18], [20]–[25].

Graph-based ANNS uses a graph index (e.g., NSG [18], HNSW [19], etc.) maintained in the memory to facilitate approximate nearest neighbors retrieval. Each vertex in a graph index represents a vector in \mathcal{X} , and an edge between two vertices defines a neighbor relationship. During the retrieval phase, a graph routing over the graph index is conducted, starting from an entry vertex and iteratively exploring the

graph index towards the query \vec{x}_q until it converges [19]. *The main limitation comes from the heavyweight memory overhead of a graph index.* The memory overhead significantly increases as \mathcal{X} increases, e.g., using HNSW for a billion-scale \mathcal{X} in 128 dimensions would consume around 800 GB memory, which largely exceeds the RAM capacity on a workstation.

Existing solutions. Many efforts have been made to alleviate the memory issue of graph-based ANNS for large-scale datasets [20], [26], [27]. The basic idea is to introduce external drives (e.g., SSD) to store high-dimensional vectors, thereby reducing memory overhead. *SPANN* [20] clusters on the dataset and uses the centroids to construct a spatial partitioning tree (SPT) that resides in memory. High-dimensional vectors within each cluster are stored on SSD. *BBANN* [26] conducts balanced clustering on the dataset and uses the clustered centroids to build a graph index maintained in memory. High-dimensional vectors within each cluster are stored on SSD. The search accuracy of the above methods is significantly affected by the coarse-grained SPT or graph index built on clustered centroids, resulting in a noticeable accuracy loss [28].

DiskANN [27]. This inspires DiskANN, a Product Quantization (PQ)-based hybrid (memory+SSD) method that aims to reduce memory overhead while ensuring a high search accuracy. It first conducts PQ for original high-dimensional vectors to obtain the quantized low-dimensional vectors, then stores a PQ index for quantized vectors in memory and a graph index for original vectors in SSD. PQ index serves for lossy distance calculations, based on which initial candidate neighbors are provided. Graph index serves for re-ranking candidate neighbors based on original vectors, which is a post-verification of lossy distances, so as to enhance the search accuracy. We refer readers to [27] and §II for more details. DiskANN has been widely deployed in the industry such as Bing search of Microsoft [29] and many follow-up works present variants of DiskANN to support their own scenarios, e.g., Filter-DiskANN for filtered search [30], OOD-DiskANN for cross-modal search [31], and Fresh-DiskANN for streaming search [32]. Although DiskANN and its variants achieve a good performance on both memory overhead and search accuracy, they all ignore the important I/O issue (frequent SSD I/O requests for candidates re-ranking) that significantly affect the queries per second (QPS). In general, the latency

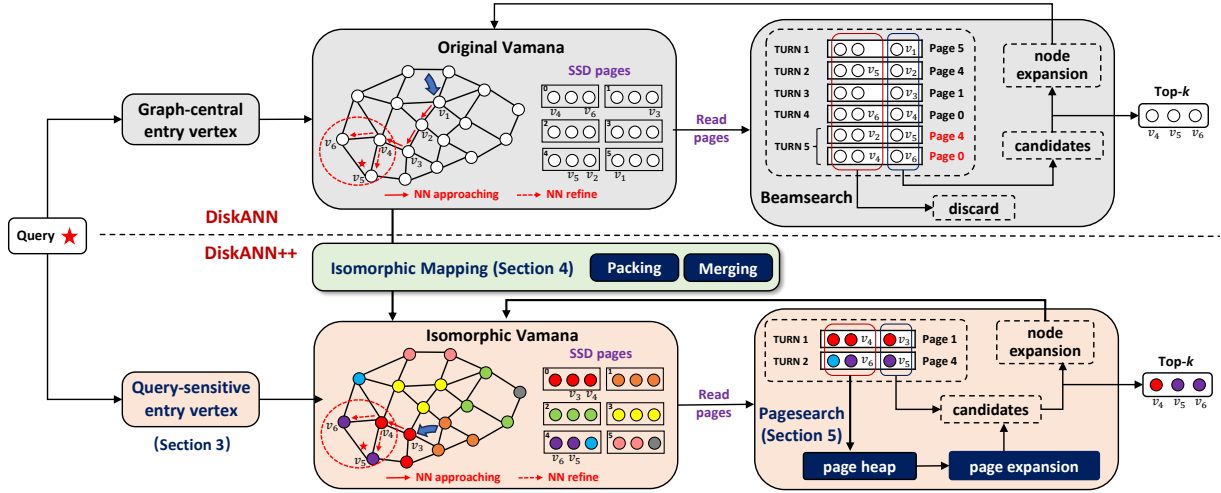


Fig. 1: Search examples on DiskANN (top) and DiskANN++ (bottom), given the same query vertex and the Vamana graph index with the same topological structure but different SSD layout.

of accessing SSD is 10X+ greater than that of accessing memory, the more the SSD I/O requests, the more the time for DiskANN. We next discuss the I/O issue of DiskANN.

I/O issue of DiskANN. Figure 1 (top) illustrates the search process of DiskANN on the Vamana graph index. Vertices in Vamana are assigned to SSD pages in a round-robin, e.g., 6 pages for 18 vertices in this example. Given a query vertex (the red star), DiskANN adopts *beamsearch* (discussed in §II) to retrieve the top- k results. It starts from the static entry vertex (i.e., the central vertex of a graph index) to explore a routing path towards query’s neighborhood. We call this the *nearest neighbor approaching* (NN approaching) phase [33]. DiskANN first reads SSD to get the Page-5 involving the entry vertex v_1 , then takes v_1 as candidate for node expansion and discard the other nodes. In the step of *node expansion*, DiskANN computes the distances between candidates’ neighbors to query and requests SSD Page-4 to obtain the closest vertex v_2 . It repeats until the search locates in the neighborhood of query (indicated by a red dashed circle). NN approaching stops when v_4 is explored. Next, DiskANN goes into the *nearest neighbor refine* (NN refine) phase to find the top- k nearest neighbors to query via a nearly brute-force vertex traversal in the query’s neighborhood, and both Page-0 and Page-4 are requested to obtain v_4 ’s two neighbors v_5, v_6 .

The I/O issue of DiskANN is two-fold: (1) *Long routing path in NN approaching phase* and (2) *Redundant I/O requests in NN refine phase*. For (1), since DiskANN takes the graph-central vertex as a static entry vertex for all queries, it would result in a long routing path in NN approaching phase, when the query is far away from the entry vertex. In above example, it needs 3 hops from v_1 to query’s neighborhood, yielding 4 SSD I/O requests out of the total 6 requests. In practice, queries often arrive randomly, which leads to a large number of long routing paths, so that affecting the overall efficiency. For (2), since DiskANN adopts a random SSD layout, it would result in redundant I/O requests in NN refine phase, when vertices on the same SSD page have less closeness in the graph index. In this example, each accessed page only involves

one useful vertex for beamsearch, reducing the data value of each I/O request and leading two redundant I/O requests of Page-0 and Page-4. Actually, they have been accessed in NN approaching phase, however, DiskANN does not know they would be required later and directly discard them as instead.

The aforementioned I/O issue inspires our study in this paper to shorten the routing path and improve the effectiveness of each I/O request (i.e., making an I/O request carry more useful vertices), so that significantly reduces the total number of I/O requests and increases the overall QPS of DiskANN.

Our solution. We next briefly introduce our solution below.

(1) **Query-sensitive entry vertex selection (§III).** For the long routing path problem, we present a query-sensitive entry vertex selection strategy to dynamically determine the entry vertex in run-time instead of the original static graph-central vertex (§III-A). Given a vector dataset \mathcal{X} and a Vamana graph built for \mathcal{X} , we first cluster the dataset to acquire N_{cluster} centroids, then we take each centroid as a query to perform ANNS on Vamana to find its top-1 nearest vertex, and finally we add all the N_{cluster} nearest vertices and the graph-central vertex into an *entry vertex candidate list*. For each incoming query \vec{x}_q , we linearly scan the candidate list and employ the nearest vertex to \vec{x}_q as the entry vertex. In Figure 1 (bottom), we may select v_3 as the entry vertex, leading a 1-hop routing path to query’s neighborhood. In §III-B, we leverage the monotonicity of MSNET [34], [35] to theoretically prove that using query-sensitive entry vertex would result in a shorter routing path than that of graph-central entry vertex. The shorter routing path usually indicates the less SSD I/O requests.

For redundant I/O issue, we present: *isomorphic mapping of graph index* and *page-level optimization to beamsearch*.

(2) **Isomorphic mapping of graph index (§IV).** Here, we propose an *isomorphic mapping on Vamana* to optimize the SSD layout. We first apply an injective mapping via *star packing* [36] on the original Vamana. It effectively assigns the vertices with great closeness into the same SSD page, so that increasing the data value of each individual I/O request. Then, we apply *bin packing* based on *First Fit Decreasing* (FFD) to make the

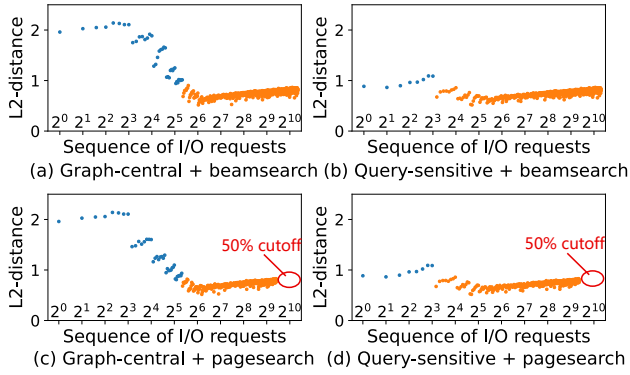


Fig. 2: Performance comparison on deep100M.

injective mapping also surjective, i.e., converting the injection to bijection (or isomorphic mapping), thereby ensuring that the original graph’s topology and addressing mode are preserved in the new SSD layout. In Figure 1 (bottom), we show the refined SSD layout with colored vertices. Note that, vertices that are close to each other are likely to be assigned to the same SSD page. Suppose we start search from v_3 and v_4 is the next-hop vertex of routing. Since they are retained in the same SSD page, we only need one SSD I/O request for Page-1 to access them simultaneously. Similarly, we only require one SSD I/O request for Page-4 to access v_5 and v_6 simultaneously.

(3) Page-level optimizations to beamsearch (§V). On the basis of the refined SSD layout above, we present a new search algorithm with page-level optimizations called *Pagesearch* as an alternative to beamsearch. The basic idea is to harness the idle CPU resources during SSD I/O requests to further mitigate the search latency. Since we apply isomorphic mapping on Vamana, each page contains more valuable vertices that would be used in the future. So, we design a novel component called *page heap* to asynchronously cache the valuable vertices from previously accessed pages. Next, we expand search from the cached valuable vertices via an asynchronous *page expansion* using the idle CPU resources while waiting the results of SSD I/O requests. The vertices obtained by page expansions would be added into the global candidates for the node expansion of beamsearch. In a nutshell, the page expansion is a complement to node expansion by providing more useful candidates from the previously accessed pages. It is a concurrent operation with SSD I/O requests without introducing extra latency.

Figure 2 shows an ablation analysis of DiskANN using beamsearch and pagesearch with static entry vertex and query-sensitive entry vertex (four combinations in total), given the same queries under the same recall@100 of 99%. The X-axis is the sequence of I/O requests and Y-axis shows the average vector distance over all accessed vertices in an I/O request to the query. We use the blue (orange) points in plot to represent the I/O requests in NN approaching (NN refine) phase. As more I/O requests are performed, the search is getting closer to the query. Figure 2 (a)-(b) show results using beamsearch with different entry vertex strategies, we found that using query-sensitive entry vertex would significantly reduce the SSD I/O requests in NN approaching phase from 32 to 8. Figure 2 (a)-

(c) show results using beamsearch and pagesearch with the same static entry vertex, we found that the SSD I/O requests in NN refine phase are reduced by at least 50%. Figure 2 (d) shows the results using pagesearch with query-sensitive entry vertex, i.e., our DiskANN++. Comparing with DiskANN (Figure 2 (a)), ours achieves a better I/O efficiency in both two phases, leading to a 2 X improvement on QPS.

Contributions. Our contributions can be concluded as follows.

- We propose a query-sensitive entry vertex selection strategy to determine entry vertex dynamically (§III-A) and prove its effectiveness theoretically (§III-B).
- We present an isomorphic mapping on Vamana to refine the SSD layout (§IV-A) and analyze its effectiveness using a metric of page compactness (§IV-B).
- We design a novel search algorithm called Pagesearch with page-level optimizations based on the refined SSD layout (§V), which utilizes idle CPU resources to update global candidates with more valuable vertices.
- Extensive experiments (§VI) conducted on eight public and commercial datasets with different types and scales, show that our solution achieves a notable QPS improvement ranging from 1.5 X to 2.2 X.

II. PRELIMINARY

Definition 1. ANNS [11]. Given a vector dataset \mathcal{X} , a query vector \vec{x}_q , and a parameter $\epsilon > 0$, the goal of ANNS is to find the top- k vectors $\{\vec{x}_1, \dots, \vec{x}_k\}$ from \mathcal{X} that are approximate nearest neighbors to \vec{x}_q . We say a vector $\vec{x}_i \in \mathcal{X}$ is an approximate nearest neighbor to \vec{x}_q if $\delta(\vec{x}_i, \vec{x}_q) \leq (1 + \epsilon) \cdot \delta(\vec{x}_i^*, \vec{x}_q)$, where $\vec{x}_i^* \in \mathcal{X}$ is the i -th nearest neighbor vector of \vec{x}_q and ϵ is an relaxation parameter controlling the top- k results’ quality.

Definition 2. Graph index. Given a vector dataset \mathcal{X} and a non-negative distance threshold $\bar{\delta}$, the graph index of \mathcal{X} w.r.t. $\bar{\delta}$ is a graph $G = (V, E)$ with the vertex set V and edge set E . (1) There is a bijection $\phi : \mathcal{X} \rightarrow V, \forall \vec{x}_v \in \mathcal{X}, \exists v \in V$ satisfying $v = \phi(\vec{x}_v)$, i.e., each vertex $v \in V$ corresponds to a vector $\vec{x}_v \in \mathcal{X}$. (2) For any two vertices $v_i, v_j \in V$ ($i \neq j$), there exists an edge $e(v_i, v_j) \in E$ iff $\delta(\vec{x}_{v_i}, \vec{x}_{v_j}) < \bar{\delta}$.

Definition 3. Recall@ k . Given a query vector \vec{x}_q , \mathcal{R}^* records the ground-truth nearest neighbors with k vectors from \mathcal{X} and \mathcal{R} records k approximate nearest neighbors returned by ANNS. Then we define the Recall@ k as follows.

$$\text{Recall@}k = \frac{|\mathcal{R}^* \cap \mathcal{R}|}{|\mathcal{R}^*|} = \frac{|\mathcal{R}^* \cap \mathcal{R}|}{k} \quad (1)$$

Definition 4. Queries Per Second (QPS). QPS is a metric indicating the number of queries that an ANNS method can handle per second. Suppose an ANNS method processes N_q queries within T seconds, then we have $\text{QPS} = N_q/T$.

Briefly introduction to DiskANN. We briefly introduce the SSD layout of the graph index and beamsearch used in DiskANN, which is important for understanding our solution.

Original SSD layout. DiskANN employs a straightforward method to store the graph index $G = (V, E)$ in SSD.

Algorithm 1: Beamsearch $(G, \vec{x}_q, B, L_s, k)$

Input: G, \vec{x}_q, B, L_s, k of top- k
Output: approximate nearest top- k neighbors \mathcal{R} to \vec{x}_q
// Initialization: lines 1-3
1 $v_e \leftarrow$ central vertex of G ; /* static entry vertex */
2 $\mathcal{C} \leftarrow \{v_e\}$; /* candidates initialized as $\{v_e\}$ */
3 $\mathcal{R} \leftarrow \emptyset$; /* top- k results initialized as \emptyset */
4 **do**
5 | $\mathcal{F} \leftarrow$ top- B unvisited vertices from \mathcal{C} for expansion ;
6 | // prepare SSD I/O requests: line 6-10
7 | $\mathcal{P} \leftarrow \emptyset$; /* page placeholders */
8 | **for** $v_i \in \mathcal{F}$ **do**
9 | | $P_j \leftarrow$ register read for page containing b_{v_i} ;
10 | | $\mathcal{P} \leftarrow \mathcal{P} \cup P_j$;
11 | **end**
12 | // SSD I/O requests: line 11
13 | read all required pages in \mathcal{P} from SSD ;
14 | // Node expansion: lines 12-15
15 | **for** $v_i \in \mathcal{F}$ **do**
16 | | $b_{v_i} = \langle \vec{x}_{v_i}, N(v_i) \rangle \leftarrow$ obtained from \mathcal{P} ;
17 | | NeighborExpansion($\vec{x}_q, b_{v_i}, \mathcal{C}, \mathcal{R}, L_s, k$) ;
18 | **end**
19 **while** $\mathcal{F} \neq \emptyset$;
20 **return** \mathcal{R} ;

Algorithm 2: NeighborExpansion $(\vec{x}_q, b_v, \mathcal{C}, \mathcal{R}, L_s, k)$

Input: $\vec{x}_q, b_v = \langle \vec{x}_v, N(v) \rangle, \mathcal{C}, \mathcal{R}, L_s, k$ of top- k
1 $\mathcal{C} \leftarrow \mathcal{C} \cup N(v)$; /* sort \mathcal{C} by PQ distance to \vec{x}_q */
2 **while** $|\mathcal{C}| > L_s$ **do**
3 | pop back from \mathcal{C} ;
4 **end**
5 $\mathcal{R} \leftarrow \mathcal{R} \cup \{\vec{x}_v\}$; /* sort \mathcal{R} by full distance to \vec{x}_q */
6 **while** $|\mathcal{R}| > k$ **do**
7 | pop back from \mathcal{R} ;
8 **end**

Definition 5. Data block. Given a vertex $v \in V$, we define the data block of v as $b_v = \langle \vec{x}_v, N(v) \rangle$, which is the basic unit for SSD storage. (1) $\vec{x}_v \in \mathcal{X}$ is the vector of v . (2) $N(v)$ recodes the identities of v 's neighbors in G . (3) We use v to indicate the identity of the data block b_v , denoted by $b_v.ID = v$.

DiskANN stores the data blocks of all $|V|$ vertices to SSD pages in a round-robin with page alignment. We use $L = \{P_1, \dots, P_n\}$ to denote the SSD layout with n pages and each $P = \{b_{v_1}, \dots, b_{v_b}\}$ contains b data blocks. For simplicity, in the rest of this paper, we use $L.IDs = \{P_1.IDs, \dots, P_n.IDs\}$ to denote the logic view of a layout that only consists of the identities of all data blocks, where $P.IDs = \{v_1, \dots, v_b\}$.

Beamsearch. Beamsearch is the core search algorithm of DiskANN, but the details are ignored in [27]. Given an SSD-resident graph index $G = (V, E)$ of the vector dataset \mathcal{X} , query vector \vec{x}_q , beam size B , search width L_s , and the size k of top- k results, Algorithm 1 shows the procedure of beamsearch. (1) It starts search from a static graph-central entry vertex $v_e \in V$ with a candidate set $\mathcal{C} = \{v_e\}$ and an empty top- k results \mathcal{R} (lines 1-3). It's worth mentioning that vertices in \mathcal{C} are ranked in ascending order of their PQ distances to \vec{x}_q using the memory-resident quantized vectors. While the vertices in \mathcal{R} are ranked in ascending order of their full distances to \vec{x}_q using the SSD-resident original vectors. (2) It chooses the unvisited top- B vertices (at most B) from \mathcal{C} , denoted by \mathcal{F} and creates

a page placeholder P_j into \mathcal{P} to register read request (line 6-10). Finally, it reads all required pages from SSD (line 11). (3) It uses all vertices from \mathcal{F} to perform node expansion (lines 12-15). The node expansion phase mainly consists of B times NeighborExpansion (Algorithm 2). NeighborExpansion uses a data block $b_v = \langle \vec{x}_v, N(v) \rangle$ to update \mathcal{C} with the neighbors $N(v)$ in ascending order of PQ distance to \vec{x}_q and ensure \mathcal{C} 's length $\leq L_s$. Then, it updates the top- k results \mathcal{R} with \vec{x}_v in ascending order of full distance to \vec{x}_q and ensure \mathcal{R} 's length $\leq k$. The re-ranking operation to \mathcal{R} is the key to guarantee the search accuracy. (4) It repeats above until no new vertex is visited and returns \mathcal{R} as the top- k results.

Problem definition. Given a vector dataset \mathcal{X} , a memory constraint M , a graph index G built for \mathcal{X} , and a query vector \vec{x}_q , DiskANN aims to maintain a PQ index within M size in memory and leverage the SSD-resident G to return the top- k approximate nearest neighbors to \vec{x}_q with a high Recall@ k .

Our goal. On this basis, our goal in this paper is: Given the conditions unchanged, we aim to design a refined SSD layout of graph index and a new search algorithm based on such layout, to retrieve the top- k results having the same Recall@ k as DiskANN, while improving the QPS by reducing the SSD I/O requests, i.e., increasing QPS without sacrificing accuracy.

III. QUERY-SENSITIVE ENTRY VERTEX

To solve the first I/O issue of DiskANN, we present a query-sensitive entry vertex selection strategy discussed in §III-A.

A. Method Overview

Offline candidate entry vertices generation. Given a vector dataset \mathcal{X} and the Vamana graph index G of \mathcal{X} , we generate the entry vertex candidates as follows. First, we employ the mini-batch-kmeans [37] to cluster \mathcal{X} into N_{cluster} clusters $\{c_1, \dots, c_{N_{\text{cluster}}}\}$. Second, we take each c_i 's centroid as an input query \vec{x}_q to find its top-1 nearest neighbor from G . Finally, we record all the nearest neighbors for N_{cluster} centroids in a linear table as the entry vertex candidates.

Online entry vertex selection. Since each candidate is a representative vertex of a partition of \mathcal{X} , it's reasonable to take it as the entry vertex when the incoming query locates in the same partition. To this end, given the candidate entry vertices and a query vector \vec{x}_q , we select a candidate entry vertex with the closest distance to \vec{x}_q as the entry vertex.

B. Theoretical Analysis of Effectiveness

We next theoretically prove that using query-sensitivity entry vertex can provide a tighter upper bound on the routing length than that of graph-central entry vertex. Since the graph index of DiskANN is developed based on Monotonic Search Network (MSNET) [27], similar to [18], we leverage MSNET's monotonicity to complete our analysis.

Definition 6. Monotonic Path. Given a graph index $G(V, E)$ for a vector dataset \mathcal{X} . Let $v_s, v_t \in V$, an l -hop path $\mathcal{P}(v_s, v_t)$ from v_s to v_t is a Monotonic Path, iff $\exists v_1, \dots, v_{l+1} \in V$ ($v_1 = v_s, v_{l+1} = v_t$) satisfying: (1) each pair of adjacent vertices in

\mathcal{P} has an edge $e(v_i, v_{i+1}) \in E$, (2) $\delta(\phi^{-1}(v_t), \phi^{-1}(v_{i+1})) < \delta(\phi^{-1}(v_t), \phi^{-1}(v_i))$, where $\phi^{-1}(v)$ denotes v 's vector $\vec{x}_v \in \mathcal{X}$ (Definition 2). This implies that the greater the number of hops (in a path) from v_i to v_t , the larger the vector distance between them. We call such a path a monotonic path $\mathcal{MP}(v_s, v_t)$.

Definition 7. Monotonic Search Network. Given a graph index $G(V, E)$ for a vector dataset \mathcal{X} . G is a Monotonic Search Network, iff $\forall v_s, v_t \in V, \exists \mathcal{MP}(v_s, v_t)$ on G .

We provide a theorem showing the relation between the entry vertex and the upper bound on a routing path's length.

Theorem 1. Given a vector dataset \mathcal{X} distributed in a unit sphere \mathcal{B} in \mathbb{R}^d , a MSNET $G(V, E)$, and a query $\vec{x}_q \in \mathcal{B}$. For query-sensitivity entry vertex, we have N_{cluster} entry vertex candidates $\{v_{c_1}, \dots, v_{c_{N_{\text{cluster}}}}\}$, where v_{c_j} is the top-1 nearest neighbor to the centroid of cluster c_j . For the static entry vertex used in DiskANN, we use v_{c_0} to denote the graph-central vertex. \vec{x}_{q^*} is the top-1 nearest neighbor of \vec{x}_q within \mathcal{X} ($v_{q^*} = \phi(\vec{x}_{q^*})$ is the vertex in G). Given above assumptions, the following inequality holds for $\exists j \in \{1, \dots, N_{\text{cluster}}\}$:

$$\overline{|\mathcal{MP}(v_{c_j}, v_{q^*})|} \leq \overline{|\mathcal{MP}(v_{c_0}, v_{q^*})|}, \quad (2)$$

where $\overline{|\mathcal{MP}(\cdot, \cdot)|}$ represents the upper bound on the length of a Monotonic Path, i.e., the number of hops.

Proof. We prove this theorem with the following two cases.

Case 1. Suppose $N_{\text{cluster}} = 1$, then we have $v_{c_1} = v_{c_0}$. This is because c_1 is the entire graph G and the central vertex of G actually is the top-1 nearest neighbor of c_1 's centroid. Thus, we have $\overline{|\mathcal{MP}(v_{c_1}, v_{q^*})|} = \overline{|\mathcal{MP}(v_{c_0}, v_{q^*})|}$.

Case 2. For $N_{\text{cluster}} > 1$, we introduce the concept of *open sphere* to derive the upper bound on a routing path's length.

Let $\mathcal{H}(\vec{x}_{q^*}, \theta)$ denotes an open sphere in \mathbb{R}^d with center \vec{x}_{q^*} and radius θ , $\mathcal{H}_{\text{vol}}(\vec{x}_{q^*}, \theta)$ denotes the volume of $\mathcal{H}(\vec{x}_{q^*}, \theta)$. Considering a monotonic path $\mathcal{MP}(v_{c_j}, v_{q^*})$ involving vertices $\{v_1, \dots, v_{l+1}, v_{q^*}\}$ ($v_1 = v_{c_j}$ is an entry vertex), for simplicity, we use the notation Vol_i to denote the volume of a sphere, i.e., $\text{Vol}_i = \mathcal{H}_{\text{vol}}(\vec{x}_{q^*}, \delta(\vec{x}_{q^*}, \vec{x}_{v_i}))$, for $i \in \{1, 2, \dots, l\}$. Since the volume of a sphere is calculated as

$$\mathcal{H}_{\text{vol}}(\cdot, \theta) = \frac{(\sqrt{\pi}\theta)^d}{\Gamma(\frac{d}{2}) + 1}, \quad (3)$$

then we have the following for $i \in \{1, 2, \dots, l\}$:

$$\frac{\text{Vol}_{i+1}}{\text{Vol}_i} = \left(\frac{\delta(\vec{x}_{q^*}, \vec{x}_{v_{i+1}})}{\delta(\vec{x}_{q^*}, \vec{x}_{v_i})}\right)^d. \quad (4)$$

We next show the relationship between $\delta(\vec{x}_{q^*}, \vec{x}_{v_{i+1}})$ and $\delta(\vec{x}_{q^*}, \vec{x}_{v_i})$. Given a cluster c_j , its diameter is $\bar{R} = \max(\delta(\vec{x}_u, \vec{x}_v))$ for $\vec{x}_u, \vec{x}_v \in c_j$. We use $R^* = \min |\delta(\vec{x}_{q^*}, \vec{x}_{v_i}) - \delta(\vec{x}_{q^*}, \vec{x}_{v_j})|$ to represent the minimum distance difference in any monotonic path $\mathcal{MP}(v_s, v_{q^*})$ from an arbitrary vertex v_s to v_{q^*} , where $v_i, v_j \in \mathcal{MP}(v_s, v_{q^*})$ for $i \neq j$. According to Definition 6, we have $\delta(\vec{x}_{q^*}, \vec{x}_{v_i}) > \delta(\vec{x}_{q^*}, \vec{x}_{v_{i+1}})$, so that $\delta(\vec{x}_{q^*}, \vec{x}_{v_i}) - \delta(\vec{x}_{q^*}, \vec{x}_{v_{i+1}}) \geq R^* > 0$ naturally holds. Thereby, due to $\bar{R} \geq \delta(\vec{x}_{q^*}, \vec{x}_{v_i}) \geq$

$\delta(\vec{x}_{q^*}, \vec{x}_{v_i}) - \delta(\vec{x}_{q^*}, \vec{x}_{v_{i+1}}) \geq R^*$, we have

$$\begin{aligned} \bar{R} \cdot (\delta(\vec{x}_{q^*}, \vec{x}_{v_i}) - \delta(\vec{x}_{q^*}, \vec{x}_{v_{i+1}})) &\geq \delta(\vec{x}_{q^*}, \vec{x}_{v_i}) \cdot R^* \\ &\Rightarrow \frac{\bar{R} - R^*}{\bar{R}} \geq \frac{\delta(\vec{x}_{q^*}, \vec{x}_{v_{i+1}})}{\delta(\vec{x}_{q^*}, \vec{x}_{v_i})}. \end{aligned} \quad (5)$$

According to Eq. 4 and Eq. 5, we have

$$\frac{\text{Vol}_{i+1}}{\text{Vol}_i} \leq \left(\frac{\bar{R} - R^*}{\bar{R}}\right)^d. \quad (6)$$

Given $\overline{\text{Vol}} = \mathcal{H}_{\text{vol}}(\vec{x}_{q^*}, \bar{R})$, we have:

$$\begin{aligned} \text{Vol}_{l+1} &\leq \text{Vol}_l \cdot \left(\frac{\bar{R} - R^*}{\bar{R}}\right)^d \\ &\leq \text{Vol}_1 \cdot \left(\frac{\bar{R} - R^*}{\bar{R}}\right)^{ld} \leq \overline{\text{Vol}} \cdot \left(\frac{\bar{R} - R^*}{\bar{R}}\right)^{ld} \\ \Rightarrow \log(\text{Vol}_{l+1}) &\leq \log(\overline{\text{Vol}}) + ld \cdot \log\left(\frac{\bar{R} - R^*}{\bar{R}}\right) \\ \Rightarrow l &\leq \frac{\log(\delta(\vec{x}_{q^*}, \vec{x}_{v_{l+1}})) - \log(\overline{\text{Vol}})}{\log(\bar{R} - R^*) - \log(\bar{R})} \triangleq f(\bar{R}). \end{aligned} \quad (7)$$

Above derivation shows the upper bound on the length of l is $f(\bar{R})$, we next analyze the monotonicity of $f(\bar{R})$ as

$$\begin{aligned} \frac{df}{d\bar{R}} &= \frac{\frac{1}{\bar{R}}[\log \bar{R} - \log(\bar{R} - R^*)]}{(\log(\bar{R} - R^*) - \log(\bar{R}))^2} \\ &\quad + \frac{(\log \bar{R} - \log \delta(\vec{x}_{q^*}, \vec{x}_{v_{l+1}}))(\frac{1}{\bar{R} - R^*} - \frac{1}{\bar{R}})}{(\log(\bar{R} - R^*) - \log(\bar{R}))^2}. \end{aligned} \quad (8)$$

Since we have the following inequalities:

- $\log \bar{R} - \log(\bar{R} - R^*) > 0$,
- $\log \bar{R} - \log \delta(\vec{x}_{q^*}, \vec{x}_{v_{l+1}}) > 0$,
- $\frac{1}{\bar{R} - R^*} - \frac{1}{\bar{R}} > 0$,

$f(\bar{R})$ is monotonically increasing. Moreover, since we assume $N_{\text{cluster}} > 1$, we have $\bar{R} \leq \frac{1}{2}$ and the following holds. \square

$$\overline{|\mathcal{MP}(v_{c_j}, v_{q^*})|} = f(\bar{R}) + 1 \leq f\left(\frac{1}{2}\right) + 1 = \overline{|\mathcal{MP}(v_{c_0}, v_{q^*})|} \quad (9)$$

C. Complexity Analysis

Complexity. The time complexity of offline candidates generation stems from the mini-batch-kmean, which is $O(r \cdot N_{\text{batch}} \cdot N_{\text{cluster}} \cdot d)$ [37], where r is the number of clustering iterations, N_{batch} is the mini-batch size, N_{cluster} is the number of entry vertices, and d is the dimensionality of a vector dominating the distance calculation's cost. The time complexity of online entry vertex selection arises from the distance calculations between each candidate and \vec{x}_q , which is $O(N_{\text{cluster}} \cdot d)$.

Remarks. (1) The efficiency improvement brought by query-sensitivity entry vertex comes from the trade-off between the time spent for online entry vertex selection (in memory) and the time saved for SSD I/O. Since reading an SSD page is at least 10 X slower than that of reading memory, it's natural that we have a good efficiency compared with DiskANN. (2) In practical, we prefer a smaller N_{cluster} to decrease the overhead of query-sensitivity entry vertex selection, when SSD's I/O bandwidth is large (or we say that SSD I/O is fast). Otherwise, a larger N_{cluster} would be better. We experimentally show N_{cluster} 's effect under diverse SSD I/O bandwidth in §VI-E.

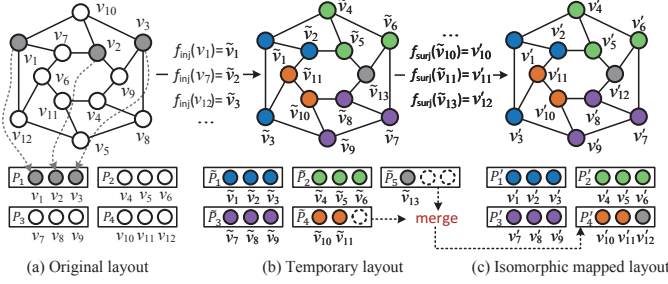


Fig. 3: Isomorphic mapping on a graph index

IV. ISOMORPHIC MAPPING ON VAMANA

In this section, we present an isomorphic mapping on Vamana to refine its SSD layout, thus increasing the data value of each SSD page (§IV-A), then analyze its effectiveness via *algebraic connectivity* [38] (§IV-B), and show its complexity (§IV-C). In §V-B, we will discuss how to use such a refined SSD layout to accelerate search via a page-based search.

A. Pack-Merge-based Method

Given the page capacity of b , DiskANN writes data blocks to SSD pages in a round-robin (Figure 3 (a)). In this way, we can quickly compute a given vertex’s resident page, yielding an efficient SSD addressing. For example, given a vertex v_i , b_{v_i} is the $i\%b$ -th data block of the $\lceil \frac{i}{b} \rceil$ -th SSD page.

We aim to refine the SSD layout by increasing the data value of each SSD page while keeping the original addressing mode unchanged. Achieving this is non-trivial. *Edge-based graph partitioning* methods [39]–[41] suffer from the redundancy in vertices, e.g., one vertex would appear multiple times in different SSD pages, invalidating original addressing mode. *Vertex-based graph partitioning* methods [42]–[44] fail to ensure that each SSD page contains the same number of vertices, also undermining the calculation of SSD offsets. *Graph reordering* method [45] keeps the addressing mode unchanged, but they load the entire graph and construct a reverse index in memory render them inapplicable to large-scale graphs. We compare our solution to representative reordering methods in §VI.

Different from them, we present a low-memory overhead, low-time complexity lightweight isomorphic mapping on Vamana, while retaining the original rapid SSD addressing mode.

Definition 8 (Isomorphic mapping). *Given two SSD layouts L and L' for graphs $G = (V, E)$ and $G' = (V', E')$. We say $f : L.IDs \rightarrow L'.IDs$ is an isomorphic mapping on their logical view (or logical layout), iff f is a bijection satisfying three conditions: (1) L and L' contain the same number of data blocks. (2) $\forall b_{v_i}, b_{v_j} \in L$, if their identities $v_i \neq v_j$, then $f(v_i) \neq f(v_j)$. (3) $\forall b_{v_i}, b_{v_j} \in L$, if $\exists e(v_i, v_j) \in E$, then $e(v'_i, v'_j) \in E'$ where $v'_i = f(v_i)$ and $v'_j = f(v_j)$.*

Figure 3(c) shows an isomorphic mapped SSD layout of a graph. Each data block b_v of $v \in V$ has a mapped $b_{v'}$ of $v' \in V'$ and all the data blocks on SSD pages retain the ascending order of vertex ID, thus we can efficiently access SSD pages using the same addressing mode as DiskANN. Since there exists various isomorphic mapping f , we need to implement one that can increase the data value of SSD pages. So, we

Algorithm 3: Packing($G, L.IDs, b$)

Input: $G, L.IDs, b$
Output: temporary logical layout $\tilde{L}.IDs$ with f_{inj}

// Initialization: line 1
1 **Visit** $\leftarrow \emptyset, \tilde{L}.IDs \leftarrow \emptyset, newID \leftarrow 1, f_{inj} \leftarrow \emptyset;$
// Star packing: lines 2-18
2 **for** $v \in V$ && $v \notin \text{Visit}$ **do**
3 **Visit** $\leftarrow \text{Visit} \cup \{v\};$
4 $\tilde{P}.IDs \leftarrow \{v\};$ /* a new temporary logical page */
5 **sort** $N(v) \subseteq V$ in ascending order of PQ distance;
// update $\tilde{P}.IDs$ with at most b vertices
6 **for** $v_i \in N(v)$ in order **do**
7 **if** $|\tilde{P}.IDs| < b$ **then**
8 $\tilde{P}.IDs \leftarrow \tilde{P}.IDs \cup \{v_i\};$
9 **Visit** $\leftarrow \text{Visit} \cup \{v_i\};$
10 **else**
11 **break** ;
12 **end**
13 **end**
14 **if** $|\tilde{P}.IDs| < b$ **then**
15 pad $\tilde{P}.IDs$ with zero ; /* page alignment */
16 **end**
17 $\tilde{L}.IDs \leftarrow \tilde{L}.IDs \cup \tilde{P}.IDs$
18 **end**
// Injection from $L.IDs \rightarrow \tilde{L}.IDs$: lines 19-26
19 **for** $\tilde{P}.IDs \subset \tilde{L}.IDs$ **do**
20 **for** $v_i \in \tilde{P}.IDs$ **do**
21 $j = newID++;$
22 $f_{inj}.put(v_i, \tilde{v}_j);$ /* update with $f_{inj}(v_i) = \tilde{v}_j$ */
23 update $\tilde{P}.IDs$ with $\tilde{v}_j;$
24 **end**
25 $newID = (\lceil \frac{newID}{b} \rceil - 1) \cdot b + 1;$
26 **end**
27 **return** $\tilde{L}.IDs$ and $f_{inj};$

present our *pack-merge-based method* to return a logical layout $L'.IDs$ with an isomorphic mapping $f : L.IDs \rightarrow L'.IDs$. It consists of two steps: packing (Algorithm 3) and merging (Algorithm 4). Packing aims to return a temporary logical layout $\tilde{L}.IDs$ by an injection f_{inj} from $L.IDs$ (Figure 3(b)) and merging aims to return a final logical layout $L'.IDs$ by a surjection f_{surj} from $\tilde{L}.IDs$. The isomorphic mapping $f = f_{surj}(f_{inj}(\cdot))$ is a bijection from $L.IDs$ to $L'.IDs$.

Packing stage. Given a graph index $G = (V, E)$ and a page capacity b , Algorithm 3 returns $\tilde{L}.IDs$ with f_{inj} by three steps.

Initialization. We initialize a set $\text{Visit} = \emptyset$ to avoid repeated visits, a temporary logical layout $\tilde{L}.IDs = \emptyset$, a vertex ID iterator $newID$ from 1, and an empty map f_{inj} (line 1).

Star packing. For each unvisited vertex $v \in V$, we add it to a temporary logical page $\tilde{P}.IDs$ and mark it as a visited vertex (lines 3-4). Then, we add v ’s $(b - 1)$ nearest neighbors (using PQ distance) from G to the same logic page $\tilde{P}.IDs$ (lines 5-13). If $N(v) < b$, we pad $\tilde{P}.IDs$ with zeros (lines 14-16). We next add $\tilde{P}.IDs$ to $\tilde{L}.IDs$ and repeat above (line 17) until all vertices have been visited. Since v and its $(b - 1)$ nearest neighbors belong to the same page, the induced graph of them is a star-derived graph. In §IV-B, we provide an effectiveness analysis using the properties of star-derived graph.

Injective mapping. Given a $\tilde{L}.IDs$, we obtain the injection f_{inj}

Algorithm 4: Merging($\tilde{L}.$ IDs, b)

Input: $\tilde{L}.$ IDs, b
Output: final logical layout $L'.$ IDs with f_{surj}
// Initialization: lines 1-2
1 $L' \leftarrow \emptyset$, newID $\leftarrow 1$, $f_{\text{surj}} \leftarrow \emptyset$;
2 sort temporary logical pages of $\tilde{L}.$ IDs in descending order of page size, i.e., the number of non-zero logical blocks;
3 **for** $\forall \tilde{P}_i.$ IDs $\subset \tilde{L}.$ IDs in order **do**
4 **if** $|\tilde{P}_i.$ IDs| == b **then**
5 $P'_i.$ IDs $\leftarrow \tilde{P}_i.$ IDs ; /* copy a logical page */
6 $\tilde{L}.$ IDs $\leftarrow \tilde{L}.$ IDs $\setminus \tilde{P}_i.$ IDs ;
7 **else**
8 // FFD-based merge: lines 8-13
9 **for** $\forall \tilde{P}_j.$ IDs $\in \tilde{L}.$ IDs in order **do**
10 **if** $|\tilde{P}_i.$ IDs| + $|\tilde{P}_j.$ IDs| $\leq b$ **then**
11 $P'.$ IDs $\leftarrow \tilde{P}_i.$ IDs + $\tilde{P}_j.$ IDs ; /* merge */
12 $\tilde{L}.$ IDs $\leftarrow \tilde{L}.$ IDs $\setminus \tilde{P}_i.$ IDs $\cup \tilde{P}_j.$ IDs ;
13 **end**
14 **end**
15 // Surjection from $\tilde{L}.$ IDs $\rightarrow L'.$ IDs: lines 15-21
16 **for** $\forall \tilde{v}_i \in \tilde{P}_i.$ IDs **do**
17 $j = \text{newID}++$;
18 $f_{\text{surj}}.\text{put}(\tilde{v}_i, v'_j)$; /* update with $f_{\text{inj}}(\tilde{v}_i) = v'_j$ */
19 update $P'.$ IDs with v'_j ;
20 **end**
21 newID = $(\lceil \frac{\text{newID}}{b} \rceil - 1) \cdot b + 1$;
22 $L'.$ IDs $\leftarrow L'.$ IDs $\cup P'.$ IDs;
23 **end**
24 **return** $L'.$ IDs and f_{surj} ;

as follows. First, for each vertex $v_i \in \tilde{P}_i.$ IDs $\subset \tilde{L}.$ IDs, we update f_{inj} with an item $f(v_i) = \tilde{v}_j$, where $j = \text{newID}$ (lines 20-24). We next update newID (line 25) and repeat above until all logical pages in $\tilde{L}.$ IDs have been visited.

Example 1. Figure 3(b) shows a temporary logical layout obtained from Figure 3(a). We use the same color to represent vertices in the same temporary page. Given the page capacity $b = 3$, we first assign v_1 and its two nearest neighbors v_7, v_{12} to the first page, pad non-full pages with zeros (e.g., the 4th and 5th pages), and repeat this until all vertices are processed. Next, we update the vertex IDs and update the injection f_{inj} with $f_{\text{inj}}(v_1) = \tilde{v}_1$, $f_{\text{inj}}(v_2) = \tilde{v}_5$, $f_{\text{inj}}(v_3) = \tilde{v}_6$, etc.

Merging stage. The temporary logical layout has one problem: some pages are not full (as we pad zeros for nodes having neighbors $< b$), and it invalidates the original addressing mode. We present a merging stage with the goal of implementing a surjection $f_{\text{surj}} : \tilde{L}.$ IDs $\rightarrow L'.$ IDs to combine data blocks from non-full pages to form a full page. Given a $\tilde{L}.$ IDs and a page capacity b , we do merging (Algorithm 4) as follows.

Initialization. We initialize a final logical layout $L'.$ IDs = \emptyset , a vertex ID iterator newID from 1, and a map f_{surj} (line 1).

FFD-based merge. We first sort temporary logical pages of $\tilde{L}.$ IDs in descending order of page size. The logical page's size is the number of non-zero logical blocks in it, denoted by $|\tilde{P}_i.$ IDs|. We retain the temporary logical pages with size = b in $L'.$ IDs (lines: 4-6 and 21) and merge others having size $< b$ to form new logical pages (lines: 8-13 and 21). Specifically,

we merge two temporary logical pages by bin packing based on First-Fit-Decreasing (FFD): we iteratively merge the largest non-full logical page with another smaller logical page to form a new full logical page until no more merge can be performed.

Surjection mapping. Given a new logical page $P'.$ IDs that is retained from $\tilde{P}_i.$ IDs (line 5) or merged by two logical pages from $\tilde{L}.$ IDs (line 10), we obtain the surjection f_{surj} as follows. For every vertex \tilde{v} from $P'.$ IDs, we update f_{surj} with an item $f_{\text{surj}}(\tilde{v}_i) = v'_j$, where $j = \text{newID}$ (lines 15-19). Next, we update newID (line 20) and add $P'.$ IDs to $L'.$ IDs (line 21). We repeat above until all logical pages from $\tilde{L}.$ IDs have been processed and return the final $L'.$ IDs with f_{surj} (line 23).

Example 2. Figure 3(c) shows the final layout obtained from Figure 3(b). We retain the first three full pages in the final logical layout. For the 4th page, it contains only two valid vertices so that we merge it with the 5th page. Then, we update the vertex IDs and update the surjection f_{surj} with $f_{\text{surj}}(\tilde{v}_{10}) = v'_{10}$, $f_{\text{surj}}(\tilde{v}_{11}) = v'_{12}$, and $f_{\text{surj}}(\tilde{v}_{13}) = v'_{12}$, etc.

Update the SSD layout using f_{inj} and f_{surj} . Given the original logical layout $L.$ IDs and the output final logical layout $L'.$ IDs with two mappings f_{inj} and f_{surj} , we update SSD layout L' with the real data blocks as follows. Given a logical page $P.$ IDs $\subset L.$ IDs, for each vertex $v_i \in P.$ IDs with data block $b_{v_i} = \langle \vec{x}_i, N(v_i) \rangle$, we first get v_i 's mapping vertex $v'_j = f_{\text{surj}}(f_{\text{inj}}(v_i))$. Then, we form $b_{v'_j}$ as $\langle \vec{x}_{v'_j}, N(v'_j) \rangle$, where $\vec{x}_{v'_j} = \vec{x}_{v_i}$ because both v_i and v'_j represent the same vertex but with different IDs. For each vertex from $N(v_i)$, we obtain its mapping vertex using $f_{\text{surj}}(f_{\text{inj}}(\cdot))$ and add it to $N(v'_j)$. Finally, we write all reformed data blocks to their corresponding positions in L' according to $L'.$ IDs.

B. Effectiveness Analysis of Refined Layout

Since our intention is to increase the data value of each SSD page, it is necessary to evaluate the compactness of an SSD page after isomorphic mapping. We present a new metric called *page compactness* based on two widely used metrics: *diameter* and *algebraic connectivity* [38]. Graph diameter is defined as the longest shortest path between any two vertices of a graph. The larger the diameter, the less the closeness between any two vertices. Given an SSD page consisting of b data blocks, we compute the diameter of the induced graph $G[V_b]$ of these b vertices by Eq. 10, where *shortest_path*(u, v) returns the length of the shortest path between u and v .

$$\text{diam}(G[V_b]) = \max_{u, v \in V_b} \text{shortest_path}(u, v) \quad (10)$$

Algebraic connectivity reflects the global connectivity of a graph. It is the second-smallest eigenvalue of the Laplacian matrix [38] of a graph. Given an induced graph $G[V_b]$ of an SSD page's b vertices, its algebraic connectivity $\lambda_2(G[V_b])$ is computed by Eq. 11, where $\text{Lap}(G[V_b])$ is the Laplacian matrix of $G[V_b]$ and ξ is the eigenvector of $\text{Lap}(G[V_b])$.

$$\lambda_2(G[V_b]) = \min_{\substack{\xi \perp \mathbf{1} \\ \xi \neq 0}} \frac{\xi^T \text{Lap}(G[V_b]) \xi}{\xi^T \xi} \quad (11)$$

TABLE I: Page compactness of two SSD layouts (original and isomorphic) for Vamana built on different datasets.

SSD layout ↓	sift100M (R32)	deep100M (R32)	turing100M (R32)
original layout	0.000004	0	0
isomorphic mapped layout	0.658033	0.560141	0.547292

Given a graph $G[V_b]$, its Laplacian matrix is computed as

$$Lap_{(i,j)}(G[V_b]) = \begin{cases} deg(v_i) & \text{if } i = j \\ -1 & \text{if } i \neq j, v_i \text{ is adjacent to } v_j \\ 0 & \text{otherwise} \end{cases} \quad (12)$$

Given above two metrics, we define page compactness as

$$\gamma(G[V_b]) = \frac{\lambda_2(G[V_b])}{diam(G[V_b])} \quad (13)$$

Note that, the smaller (larger) the diameter (algebraic connectivity), the greater the page compactness. Table I provides the page compactness of the original SSD layout and isomorphic mapped SSD layout of the Vamana built on three datasets using the same $R = 32$. In DiskANN, R is the largest out-degree of Vamana used to control the index construction. Since DiskANN assigns data blocks on SSD in a round-robin, vertices in an SSD page are almost disconnected in Vamana. As a result, many SSD pages' algebraic connectivity is close to zero, resulting in a high probability that the page compactness tends to zero. For ours, we assign a vertex's $b - 1$ nearest neighbors to the same page, so that the induced graph of them is a typical star-derived graph. Given this premise, we prove that the page compactness of ours must > 0.5 in Theorem 2.

Definition 9. Star-derived Graph. Given a graph $G = (V, E)$ with one central vertex $v \in V$ and other $|V| - 1$ peripheral vertices $V \setminus v$. We call G a star graph if all peripheral vertices have edges to v but no edges among themselves. Given another graph $G' = (V, E')$ with the same vertices as G and $E' \supset E$, G' is a star-derived graph, i.e., derived from a star graph G .

Theorem 2. Given an SSD page of the isomorphic mapped layout of Vamana, its page compactness must > 0.5 .

Proof. A star graph's diameter is fixed to 2 and its algebraic connectivity is constantly at 1. Since a star-derived graph allows connections among peripheral vertices, it may decrease the diameter (i.e., a diameter $diam(\cdot) \leq 2$) and it would certainly increase the algebraic connectivity (i.e., $\lambda_2(\cdot) > 1$). As a result, the page compactness must > 0.5 . \square

C. Complexity Analysis

Complexity. The complexity arises from both packing and merging. Assuming that basic arithmetic operations can be performed in $O(1)$ time, the complexity of packing is $O(|V| \cdot R \cdot d)$, where V is the node set of a graph G , R is the largest out-degree, and d is the dimensions. This is because we need to calculate the PQ distances between each $v \in V$ and its R neighbors and select the nearest $b - 1$ neighbors to form an SSD page. The complexity of merging is evidently $O(b \cdot N)$. So, the overall time complexity of the mapping is $O(|V| \cdot R \cdot d + b \cdot N)$.

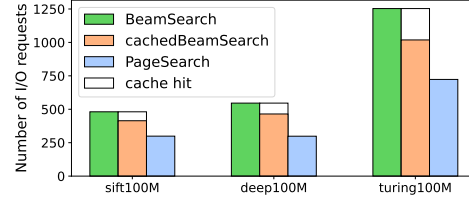


Fig. 4: The number of I/O requests (SSD I/O and cache I/O) of beamsearch, cachedBeamsearch, and pagesearch.

V. PAGE-BASED SEARCH

We next discuss how to use the refined SSD layout of isomorphic mapped Vamana to accelerate the beamsearch. Straightforwardly, we can cache all the read SSD pages and check them before requesting SSD pages to avoid redundant SSD I/Os. It's worth mentioning that this would not reduce the total number of I/O requests but only replace a part of SSD I/O requests with cache I/O requests. The greater the cache hit rate, the larger the QPS is achieved. We implemented this method called cachedBeamsearch and compare it with beamsearch. Figure 4 shows that cachedBeamsearch has the same number of I/O requests as beamsearch, of which only 10%-20% I/O requests are hit in cache and most of the cached SSD pages are unused for the node expansion of beamsearch. Moreover, the CPU remained largely underutilized during the search process due to the passive nature of cache requests. In order to take the advantages of refined SSD layout, we propose an active filtering-based asynchronous page expansion as a complement to node expansion, thus forming a new pagesearch.

Figure 5 illustrates the pipelines of our pagesearch and beamsearch. Pagesearch relies on a meticulously customized page cache pool called page heap (§V-A). It involves four basic operators: *Cache()*, *Update()*, *Check2ret()*, and *Pop()* (the green components in Figure 5(b)), based on which we design a page expansion strategy to actively filter more useful vertices as candidates for node expansion. Besides, we leverage the CPU's stall cycle (shown in Figure 5(a)) to perform the proposed page expansion asynchronously, when the SSD I/O requests are processing at the same time. In this way, we improve the CPU utilization so as to improve overall QPS. Figure 4 shows that pagesearch (right bar) achieves nearly 50% reduction of SSD I/O requests compared with beamsearch.

A. Page Heap

PageHeap is a page cache pool with four basic operators.

- **Cache()**. It caches a 4k-aligned page into the memory pool and register vertices of a page into a circular queue.
- **Update()**. It first calculates the full vector distance between each vertex in a circular queue and a query. Then, it updates a min-heap with these vertices using the above distances and remove them from circular queue. This min-heap would be used in the page expansion (see §V-B).
- **Check2ret()**. It checks whether a given page's data block exists in the memory pool. If the data block is found, it is returned as the output, otherwise it reports none.
- **Pop()**. It popups the top-1 vertex having the minimum distance to the given query, from the min-heap.

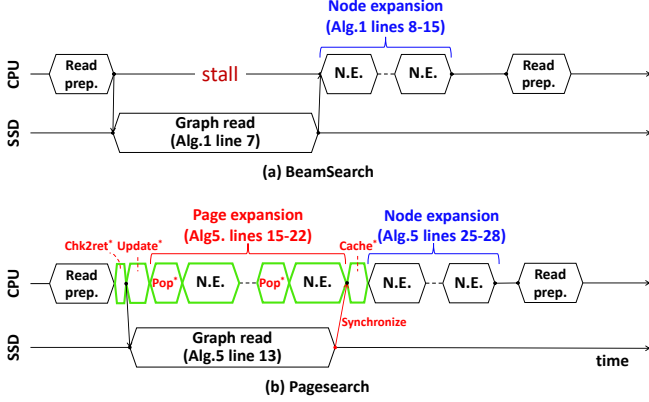


Fig. 5: Pipeline of original beamsearch and our pagesearch.

Algorithm 5: Pagesearch($G, \vec{x}_q, v_e, B, L_s, k$)

```

Input:  $G, \vec{x}_q, v_e, B, L_s, k$  of top- $k$ 
Output: approximate nearest top- $k$  neighbors  $\mathcal{R}$  to  $\vec{x}_q$ 
1  $\mathcal{C} \leftarrow \{v_e\}$ ; /* candidate set initialized as  $\{v_e\}$  */
2  $\mathcal{R} \leftarrow \emptyset$ ; /* top- $k$  results initialized as  $\emptyset$  */
3  $\mathcal{H} \leftarrow \emptyset$ ; /* PageHeap initialized as  $\emptyset$  */
4 do
5    $\mathcal{F} \leftarrow$  top- $B$  unvisited vertices from  $\mathcal{C}$  for expansion ;
6   // prepare for SSD I/O requests: lines 6-12
7    $\mathcal{P} \leftarrow \emptyset$ ; /* page placeholders initialized as  $\emptyset$  */
8   for  $v_i \in \mathcal{F}$  do
9     if  $\mathcal{H}.\text{check2ret}(v_i)$  is none then
10       $P_j \leftarrow$  register read for page containing  $b_{v_i}$  ;
11       $\mathcal{P} \leftarrow \mathcal{P} \cup P_j$  ;
12    end
13  // async SSD I/O requests: line 13
14  async read all pages in  $\mathcal{P}$  from SSD ;
15   $\mathcal{H}.\text{update}()$  ;
16  // async page expansion: lines 15-22
17  while  $b_{v_i} = \langle \vec{x}_{v_i}, N(v_i) \rangle \leftarrow \mathcal{H}.\text{pop}()$  is not none do
18    if  $v_i$  is unvisited then
19      NeighborExpansion( $\vec{x}_q, b_{v_i}, \mathcal{C}, \mathcal{R}, L_s, k$ ) ;
20      if async read done then
21        break ;
22      end
23    end
24  wait for async read done ;
25   $\mathcal{H}.\text{cache}(\mathcal{P})$  ;
26  // node expansion: lines 25-28
27  for unvisited  $v_i \in \mathcal{F}$  do
28     $b_{v_i} = \langle \vec{x}_{v_i}, N(v_i) \rangle \leftarrow \mathcal{H}.\text{check2ret}(v_i)$  ;
29    NeighborExpansion( $\vec{x}_q, b_{v_i}, \mathcal{C}, \mathcal{R}, L_s, k$ ) ;
30  end
31  return  $\mathcal{R}$ 
32 while  $\mathcal{F} \neq \emptyset$ ;

```

B. Pagesearch

Given a graph index $G = (V, E)$ of the vector dataset \mathcal{X} , a query vector \vec{x}_q , beam size B , search width L_s , and k of top- k results, Algorithm 5 shows the entire procedure.

Initialization. We initialize the candidate set \mathcal{C} as $\{v_e\}$, the top- k results $\mathcal{R} = \emptyset$, and the page heap $\mathcal{H} = \emptyset$ (lines 1-3).

Read Preparing. We prepare SSD I/O requests for unvisited top- B vertices from \mathcal{C} , denoted by \mathcal{F} . (1) For each $v_i \in \mathcal{F}$, we invoke $\text{check2ret}()$ to check if v_i is cached and register a page placeholder P_j into \mathcal{P} (lines 6-12). (2) We submit the

TABLE II: Statistics of datasets

Dataset	Dimension	LID [46]	Query	Base (M:10 ⁶ , B:10 ⁹)
image ¹	100	15.3	10,000	100M
sift [47]	128	16.6	10,000	100M
deep [48]	96	17.6	10,000	10M~1B
msong [49]	420	18.0	200	0.99M
crawl [50]	300	27.4	10,000	1.99M
turing [51]	100	30.5	100,000	100M
glove-100 [52]	100	34.3	10,000	1.18M
gist [47]	960	35.0	1,000	1M

prepared read requests asynchronously (line 13).

Page Expansion. During asynchronous reading, we $\text{Update}()$ page heap (line 14) and begin page expansion. We iteratively $\text{Pop}()$ one vertex from page heap and invoke NeighborExpansion (Algorithm 2) to update both \mathcal{C} and \mathcal{R} with more promising candidates (lines 15-22). We terminate the page expansion when asynchronous SSD read completes (lines 18-20), making it synchronized with the asynchronous read.

Node Expansion. When page expansion finishes, we execute the same node expansion as beamsearch: taking unvisited node's data block b_{v_i} from the memory pool of page heap by invoking $\text{check2ret}()$, for further NeighborExpansion .

Pagesearch repeats the above read preparing, page expansion, and node expansion until no more vertices are visited (line 30) and returns the top- k results \mathcal{R} (line 29).

VI. EVALUATION

We evaluate our DiskANN++, DiskANN, and other competitors on eight large-scale datasets, to answer five questions: **Q1:** Does DiskANN++ achieve a better QPS vs. recall@ k than others within a low memory footprint (§VI-B)?

Q2: Does DiskANN++ consistently outperform DiskANN under various hardware resource constraints (§VI-C)?

Q3: How's the scalability of DiskANN++ w.r.t. different datasets (with various hardness) and data scales (§VI-D)?

Q4: What's the parameter sensitivity of DiskANN++ (§VI-E)?

Q5: What is the contribution of each component individually or in combination to DiskANN++ (§VI-F).

A. Experiment Settings

Datasets. Table II shows statistics of eight datasets, including seven public datasets (msong [49], glove-100 [52], crawl [50], gist [47], sift [47], deep [48], and turing [51]) and one commercial dataset (image¹). The slices of deep ranging from 1M to 1B were employed to evaluate the stability at scales.

Comparing Algorithms. We compared with three SSD-based solutions: (1) SPANN [20]. (2) BBANN [26]. (3) DiskANN [27]. For ours, we implemented three versions: (4) DiskANN++ (w/o compression), (5) DiskANN++ (sq16), and (6) DiskANN++ (sq8). Here, sq16 and sq8 are compression ratio that means we compress a vector from fp32 to int16 or int8. The larger the number, the smaller the compression ratio. We study the effect of compression on DiskANN++ in §VI-B.

Resource Constraints. We default to employing 10% of the dataset size as the memory constraint and use 8 threads for search (one thread per query). This configuration enables full usage of I/O resources when disk bandwidth and IOPS are

¹Commercial image dataset provided by Huawei Technologies Co., Ltd.

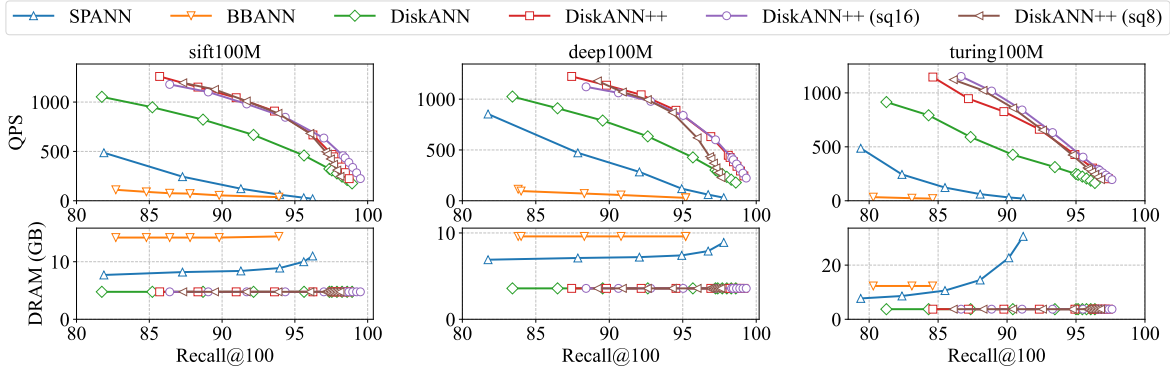


Fig. 6: QPS and DRAM usage vs. Recall@100 for SPANN, BBANN, DiskANN, and DiskANN++ (with sq16/sq8 compression)

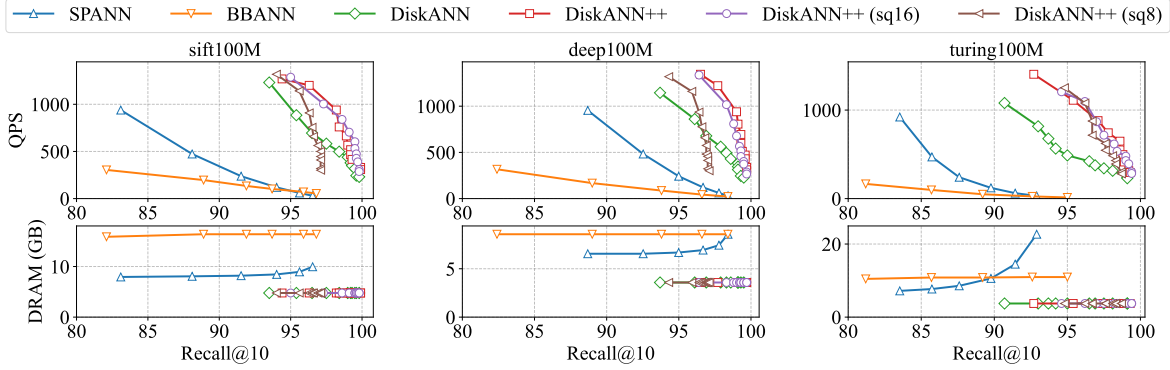


Fig. 7: QPS and DRAM usage vs. Recall@10 for SPANN, BBANN, DiskANN, and DiskANN++ (with sq16/sq8 compression)

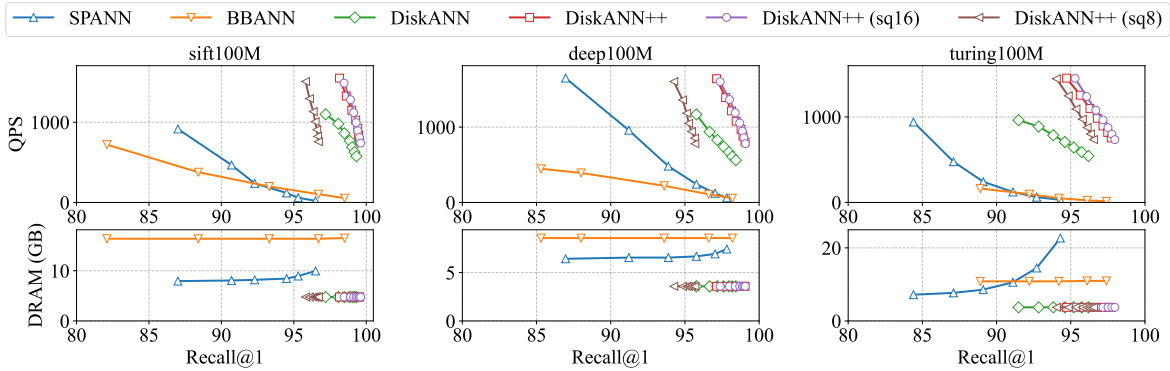


Fig. 8: QPS and DRAM usage vs. Recall@1 for SPANN, BBANN, DiskANN, and DiskANN++ (with sq16/sq8 compression)

not restricted. We also conducted experiments under varying hardware conditions (§VI-C) via Docker, including 1 to 8 threads (i.e., running 1 to 8 queries concurrently), 4k random I/O bandwidth (100-700MB/s), and 1-25% of the dataset size as memory constraints.

Evaluation Metrics. We evaluate ANNS’s effectiveness by *recall@k* ($k = 1, 10, 100$). We evaluate ANNS’s efficiency by *QPS* and *speedup*. QPS exhibits an inverse correlation with each query’s runtime. Speedup is defined as the ratio of QPS achieved by DiskANN++ and DiskANN at the same recall@ k .

Implementation Setup. For SPANN, BBANN, and DiskANN, we use public implementations provided in their GitHub repositories [53]–[55]. All algorithms were compiled in C++17, retaining relevant SIMD and prefetching instructions. The benchmark scripts were implemented using Bash and Python3.

All experiments were conducted on an Ubuntu 20.04 server with CPU-10C20T 3.70GHz, SSD-PM981 2TB, DRAM-32GB 2133Mb/s DDR4 x4.

Parameter Settings. In both DiskANN and DiskANN++, we utilize identical graph construction parameters: $R=32$, $L=500$, $\alpha_1=1.0$, $\alpha_2=1.2$, and the same PQ construction method: 8-bit encoding (i.e., 256 pivots per chunk). The DRAM limit of index construction is set to 64GB, while in the index optimizing and searching stage, the DRAM limit are 10% of the dataset size. Under such memory constraints, the construction of the index for 1 billion-sized slices is conducted in 10 slices and then merged, following the method outlined in the original DiskANN paper. In BBANN, we adopt index construction parameters based on the recommended configurations in its GitHub repository, with slight modifications: HNSW max

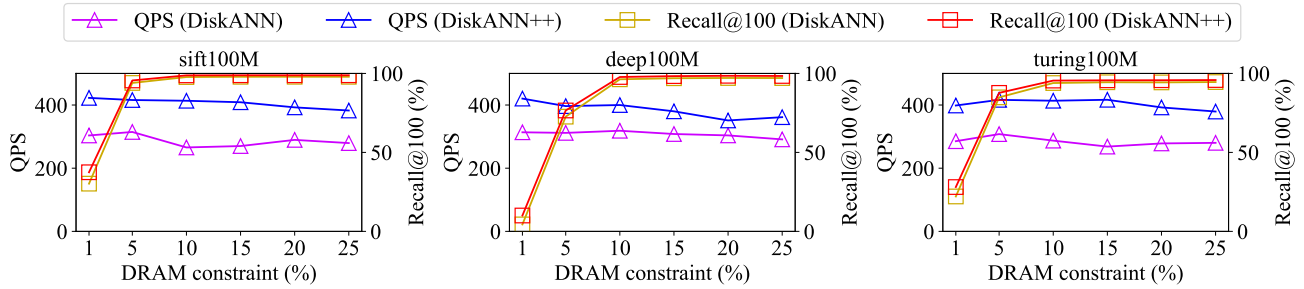


Fig. 9: Effect of memory constraint on QPS and recall@100 of DiskANN and DiskANN++.

layers is set to 32, candidate set list’s size in construction is set to 512, and block size is 4096KB. In SPANN, we directly adopt the recommended parameter configuration it provides.

B. Effectiveness and Efficiency Evaluation

We set the same memory constraint (10% of the dataset size) for DiskANN and DiskANN++. For SPANN and BBANN, since they require at least 20% of the dataset size in memory to gain an acceptable recall (>85%) with recommended parameters, we set the memory constraint for them as 20%.

QPS vs. recall@k. Figure 6-8 (top) demonstrate that DiskANN family of algorithms strikes a better balance between QPS and recall than that of SPANN and BBANN. DiskANN++ achieves a 50%-100% improvement trend under the same recall@k. For example, given the same recall@100 as 97% in deep100M, the QPS of DiskANN++ and DiskANN are 605.3 and 310.2, leading a 95% improvement on QPS. The same improvement hold for recall@1 and recall@10 as well. In compression scenarios, DiskANN++ (sq16) shows the similar trends as that without compression. Besides, the sq16 compression slightly improves the QPS given the same recall@k. This is because it reduces the word length of node data by compressing vector with less precision loss, which allows for accommodating more nodes in each SSD page. Consequently, it increases the page expansion width (i.e., *b*) in pagesearch to a certain extent, thus accelerating the convergence speed of searching. On the other hand, we found that a noticeable drop occurs at high recall for sq8. This is because the significant precision loss of original vector when a strong compression is conducted.

Memory Usage. As shown in Figure 8-6 (bottom), SPANN and BBANN consume more memory than DiskANN family of algorithms and the memory usage increases as the precision increases. The reason is two-folded: (1) SPANN and BBANN inevitably require reading more disk clusters to achieve higher precision, resulting in ever-increasing memory consumption, and (2) SPANN and BBANN maintain SPT or graph index in memory, which inherently require more memory. In contrast, the DiskANN family of algorithms maintain a stable memory footprint that is lower than others because the PQ is used to obtain low-dimensional quantized vectors resident in memory.

C. Effect of Hardware Resources

Effect of I/O limits and # threads. We first study the effect of hardware resources on DiskANN++ at a high recall@100 of

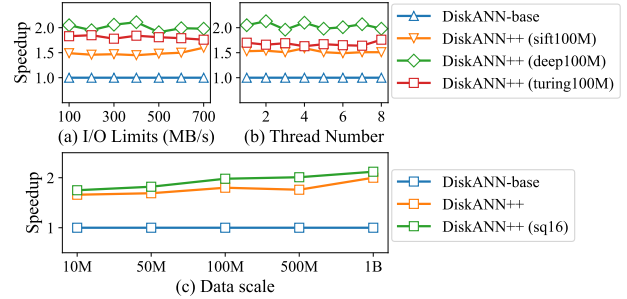


Fig. 10: Speedup of DiskANN++ of different (a) I/O bandwidth, (b) # thread, and (c) dataset scale (deep: 10M~1B).

97% on deep100M, sift100M, and turing100M, under varying I/O bandwidth (Figure 10(a)) and # threads (Figure 10(b)). From Figure 10(a)-(b), we found that DiskANN++ achieves consistent speedup across varying I/O limits and # threads (one thread per query) on the same dataset. The differences of speedup across datasets is attributed to the impact of different vector dimensions and local intrinsic dimensionality (LID) on search lengths, as discussed in [56].

Effect of DRAM usage constraints. We study the impact of memory constraints on the QPS and recall@k. We provide results with fixed search parameters under memory constraints at 1%-25% of the dataset size, e.g., the total size of sift100M is 48GB, deep100M is 36GB, and turing is 37GB. As shown in Figure 9, DiskANN++ consistently achieves higher recall than DiskANN under various memory constraints. Additionally, it demonstrates higher search speed (note the QPS curves). We analyze that, within the DiskANN framework, the primary impact of memory constraints lies in the compression ratio of the PQ in memory, reflecting the loss of precision in the original vectors. The larger the memory constraint, the less the PQ precision’s loss. This directly influences the direction selection at each hop during search. Lower PQ quality can result in longer routing search paths. Worse still, it may lead to the search being unable to correctly reach the query’s neighbors, thereby failing to meet the desired recall requirements. From the results shown in Figure 9, we can conclude that the recall increases as memory constraint increases.

D. Scalability Evaluation

We evaluated the scalability of DiskANN++ across different data scales (Figure 10(c)) and types of datasets (Table III) given recall@100 of 97%. In Figure 10(c), the speedup is stable as the data scale increases. It is attributed to the adaptability

TABLE III: QPS and speedup results of different datasets

Datasets ↓		DiskANN	DiskANN++	DiskANN++ (sq16)		
dataset	LID	QPS	QPS	speedup	QPS	speedup
image	15.3	77.53	117.07	1.51x	143.57	1.85x
sift100M	16.6	354.1	523.32	1.48x	599.18	1.69x
deep100M	17.6	310.24	605.31	1.95x	617.77	1.99x
msong	18.0	435.99	653.35	1.50x	829.48	1.90x
crawl	27.4	738.2	1209.03	1.64x	1318.63	1.79x
turing100M	30.5	110.70	270.65	2.44x	289.77	2.61x
glove-100	34.3	90.66	245.49	2.71x	278.83	3.08x
gist	35.0	348.32	347.7	1.00x	474.93	1.36x

TABLE IV: Effect of $N_{cluster}$ on speedup under different I/O bandwidth (varied from 100 MB/s to 700 MB/s).

$N_{cluster}$ ↓	I/O bandwidth (MB/s)						
	100	200	300	400	500	600	700
4096	1.176x	1.065x	1.085x	1.189x	1.127x	1.213x	1.221x
8192	1.156x	1.086x	1.126x	1.132x	1.175x	1.305x	1.166x
16384	1.180x	1.113x	1.190x	1.237x	1.219x	1.334x	1.147x
32768	1.189x	1.159x	1.225x	1.354x	1.418x	1.238x	1.077x
65536	1.240x	1.161x	1.223x	1.275x	1.153x	1.124x	0.915x

of graph index to various data scales. Some classical studies [18], [19] have indicated that the time complexity of graph search is logarithmic which grows slowly with the increase of data scale. From Table III, ours achieves at least 1.5X speedup on most of the datasets except gist, due to its high vector dimensionality of 960, which results in only one vertex per page, limiting the effectiveness of pagesearch. However, after augmenting the node capacity to 2 with node compression of sq16, we achieved 1.36x improvement. We also noticed that our DiskANN++ is scalable to the hardness of datasets. For turing100M and glove-100 datasets that have a LID > 30 (with a modest dimensionality of 100), we achieve at least 2.44x speedup. This is because when searching on the dataset with a larger LID, NN refine phase constitutes a larger proportion and our pagesearch can effectively reduce the I/O requests.

E. Parameter Sensitivity

Effect of $N_{cluster}$. The cluster size $N_{cluster}$ has a significant impact on query-sensitive entry vertex selection strategy. So, we study its influence in Figure 11. We found that increasing $N_{cluster}$ can effectively reduce routing hops and improve the QPS, which aligns with the conclusion in Theorem 1 (§III-B). However, the search performance does not infinitely improve as $N_{cluster}$ increases. This is because the time spent in entry vertex selection cannot be ignored. For example, using an excessively large $N_{cluster} = 2^{16}$ would increase the time on entry vertex selection, leading to a bad search performance. Therefore, it is necessary to carefully adjust $N_{cluster}$ to achieve a favorable trade-off. Furthermore, as search precision (recall@100) increases, the QPS improvement brought by query-sensitive entry vertex selection diminishes. This is because the routing procedure requires more time in NN refine step than NN approaching step to find the top- k with a high recall, thus weakening the improvement brought by query-sensitive entry vertex selection. We also study the effect of $N_{cluster}$ on speedup under different I/O bandwidth (Table IV). It demonstrates that a smaller $N_{cluster}$ is preferred to decrease the overhead of online entry vertex selection, when SSD’s I/O bandwidth is large (or SSD I/O is fast). Otherwise, a larger

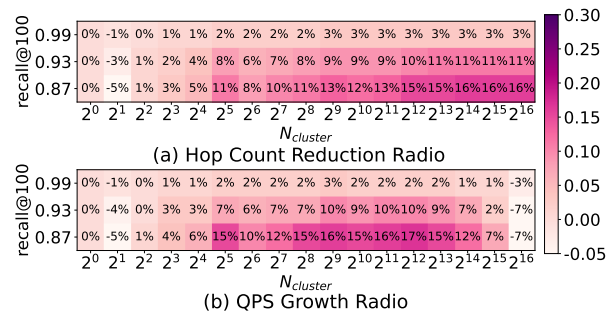


Fig. 11: Effect of the query-sensitive entry vertex (with different $N_{cluster}$) under different recall@100 (deep100M).

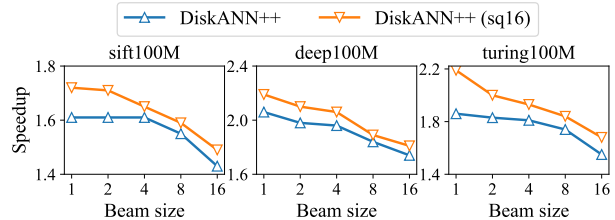


Fig. 12: Effect of beamsize B on speedup (deep100M).

$N_{cluster}$ is better. Moreover, we tested the improvement in QPS under the maximum achievable bandwidth (with $N_{cluster} = 4096$). We found that query-sensitive entry vertex strategy only consumes 0.04% of the memory usage and 0.64% of the runtime, but also offers a 1.12X speedup in QPS.

Effect of beam size B . In Figure 12, speedup decreases as the beam size increases. This is because increasing the beam size explicitly expands the width of node expansion, allowing node expansion to process more data blocks from page heap in each iteration, resulting in fewer unprocessed data blocks in page heap can be used for page expansion. However, as mentioned in the original DiskANN paper, continuously increasing the beam size is not conducive to load balancing for SSD across different queries (the original paper suggests $B = 2, 4, 8$ for better performance). Therefore, under such parameter settings, DiskANN++ still exhibits at least 1.5X speedup.

F. Ablation Analysis

Effect of each component. We employ ablation analysis to assess the contributions of query-sensitive entry vertex (A), isomorphic mapping (B), and pagesearch (C) individually within DiskANN++. The experiments compare DiskANN++ and DiskANN across QPS, mean # I/Os, and mean routing length (i.e., hops), given recall@100=97% (high recall) and recall@100=85% (low recall), across three common datasets: sift100M, deep100M, and turing100M. From Table VI, we conclude that: (1) The query-sensitive entry vertex has a modest contribution at high recall and a more substantial impact at low recall. And its contribution is independent of other components. For enhanced persuasiveness, we record the hop reduction attributed to the query-sensitive entry vertex for each query in the official query set of deep [48] (refer to Figure 13). The left subfigure illustrates the relationship between the hop reduction and the distance between the query and central vertex (medoid) of graph index, and the right subfigure

TABLE V: Overhead and speedup (at recall@100=97%) of randomOrder, parallelGorder, pack-merge (ours) using pagesearch.

graph index	DRAM usage (GB)			Runtime (sec)			Speedup with pagesearch		
	randomOrder	parallelGorder	pack-merge	randomOrder	parallelGorder	pack-merge	randomOrder	parallelGorder	pack-merge
Vamana (sift100M R32)	2.2	75.1 (MLE)	6.3	449.5	2739.1	222.3	1.02x	1.84x	1.69x
Vamana (deep100M R32)	1.9	72.5 (MLE)	5.1	381.2	2651.4	123.1	1.08x	2.15x	2.02x
Vamana (turing100M R32)	2.0	73.4 (MLE)	6.1	366.7	2644.8	195.2	1.08x	2.08x	1.88x

TABLE VI: Ablation analysis on query-sensitive entry vertex (A), isomorphic mapping (B), and pagesearch (C).

Dataset	Recall@100=85%			Recall@100=97%		
	DiskANN++					
components	QPS	mean I/Os	mean hops	QPS	mean I/Os	mean hops
-	946.42 (1.00x)	181.54	24.66	385.88 (1.00x)	447.49	57.61
A	1033.64 (1.09x)	164.57	22.51	401.14 (1.04x)	431.58	55.62
B	959.8 (1.01x)	181.54	24.66	387.17 (1.00x)	447.49	57.61
C	1065.09 (1.13x)	179.24	24.38	440.34 (1.14x)	438.87	56.6
AB	1022.24 (1.08x)	164.57	22.51	397.41 (1.03x)	431.58	55.62
AC	1152.38 (1.22x)	163.79	22.41	447.22 (1.16x)	425.35	54.92
BC	1281.32 (1.35x)	148.32	20.58	660.6 (1.71x)	291.85	38.25
ABC	1412.35 (1.49x)	133.41	18.72	691.88 (1.79x)	278.65	36.62

Dataset	Recall@100=85%			Recall@100=97%		
	DiskANN++					
components	QPS	mean I/Os	mean hops	QPS	mean I/Os	mean hops
-	945.69 (1.00x)	184.15	25.06	308.78 (1.00x)	557.93	71.42
A	1104.46 (1.17x)	153.7	21.25	325.66 (1.05x)	529.26	67.91
B	928.85 (0.98x)	184.15	25.06	305.81 (0.99x)	557.93	71.42
C	1043.07 (1.10x)	177.15	24.19	332.42 (1.08x)	549.1	70.37
AB	1096.92 (1.16x)	153.7	21.25	324.25 (1.05x)	529.26	67.91
AC	1156.4 (1.22x)	153.66	21.23	340.15 (1.10x)	528.33	67.74
BC	1296.92 (1.37x)	142.83	19.92	588.93 (1.91x)	316.78	41.42
ABC	1523.41 (1.61x)	118.89	16.99	625.23 (2.02x)	291.78	38.28

Dataset	Recall@100=85%			Recall@100=97%		
	DiskANN++					
components	QPS	mean I/Os	mean hops	QPS	mean I/Os	mean hops
-	866.13 (1.00x)	202.21	27.22	136.12 (1.00x)	1244.34	157.5
A	990.49 (1.14x)	174.84	23.79	140.21 (1.03x)	1215.26	153.81
B	855.86 (0.99x)	202.21	27.22	136.33 (1.00x)	1244.34	157.5
C	988.52 (1.14x)	189.56	25.57	153.48 (1.13x)	1203.58	152.33
AB	958.94 (1.11x)	174.84	23.79	139.33 (1.02x)	1215.26	153.81
AC	1066.85 (1.23x)	173.12	23.58	155.43 (1.14x)	1187.15	150.33
BC	1228.52 (1.42x)	152.59	21.07	259.17 (1.90x)	714.63	91.37
ABC	1363.68 (1.57x)	131.89	18.54	265.95 (1.95x)	694.09	88.84

provides a statistical overview of the query count for different hop reduction. It is evident that queries positioned farther from the medoid experience more substantial benefits. Practically, there is a higher probability of a random high-dimensional point falling at a greater distance compared to falling near a fixed point. Hence, on average, queries exhibit a pronounced reduction in hop count. (2) Using isomorphic mapping alone does not accelerate beamsearch, because beamsearch doesn't have a mechanism to consider the highly-related vertices in the same page. Remark: despite the potential increase in CPU cache prefetching effects (refer to [45]), in scenarios related to disks in this context, SRAM prefetch optimization is diluted to insignificance by a larger and slower proportion of I/O operations. (3) Using pagesearch alone shows a limited improvement. This is because the original SSD layout is established by a round-robin assignment, resulting a low locality of vertices in the same page. So, pagesearch cannot benefit more from original SSD layout. (4) The combination of isomorphic mapping and pagesearch represents the primary contribution, it brings more improvement on QPS at higher recall. This is because pagesearch can effectively unleash the potential of the refined SSD layout via isomorphic mapping.

Effect of different graph reordering methods. The key of our isomorphic mapping is the pack-merge method (§IV-A). We replace it by different graph reordering methods that can

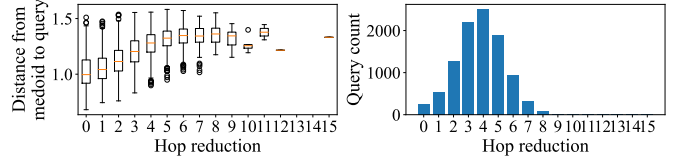


Fig. 13: Relationship between the hop reduction and the distance between the query and graph medoid (left). Query count for different hop reduction (right).

also be used to refine the SSD layout, e.g., *randomOrder* and *Gorder* [45], and evaluate their overhead (memory usage and runtime) and speedup, using the same pagesearch. Considering the immense time complexity of *Gorder*, rendering it impractical to complete in a foreseeable time, we adopted the improved *parallelGorder* method used in *OOD-DiskANN* [31]. This method sacrifices some reorder effect to enhance runtime speed. All requirements are conducted with 8 threads.

From Table V, we found that our pack-merge method is the most efficient one that consumes modest memory and offers a comparable QPS improvement as *parallelGorder*+pagesearch. In contrast, since *parallelGorder* requires > 70GB memory to perform, which largely exceeds the memory constraint (MLE stands for memory limit exceed), its practical deployability is significantly limited. Therefore, due to the lightweight nature of the pack-merge-based method, we can easily optimize the existing Vamana index on any device where *DiskANN* is deployed, whether it is the machine used for index construction or the one used for searching. This optimization can lead to a substantial improvement in search performance.

VII. RELATED WORK

We review the relevant technologies, including ANNS, graph-based ANNS, and *DiskANN* and its variants.

Approximate nearest neighbor search (ANNS). The researches of ANNS are generally categorized as three types: quantization-based [57]–[61], hash-based [12], [13], [62]–[65], and graph-based [18], [19], [66]–[68] ANNS. Among them, graph-based methods achieve a favourable tradeoff between accuracy and efficiency [11], [21], [23], [24]. However, existing research has primarily focused on optimizing search accuracy and efficiency but ignore the significant memory overhead for maintaining the large graph index. This motivates the following disk-resident graph-based ANNS.

Disk-resident graph-based ANNS. Most of the solutions are based on hybrid indexing schemes that utilize both disk and memory. *GRIP* [69] reduces the memory consumption of a graph index by compressing high-dimensional vectors to lower-dimensional ones. *HM-ANN* [70] addresses memory challenges via heterogeneous storage solutions. *SPANN* [20] is a partition tree-based method that maintains a small SPT in memory but the full vectors in disk. *BBANN* [26] combines

a memory resident invert index and on-disk graph index to optimize search tasks. The search accuracy of above methods is affected by the compressed vectors, low-quality invert index, and SPT. So, researchers resort to DiskANN family of methods to reduce memory overhead while ensuring a high accuracy.

DiskANN family of methods. DiskANN [27] introduces PQ to assist graph-based ANNS and memory usage. It has been widely deployed in the industry such as Bing search of Microsoft [29] and many follow-up works present variants of DiskANN, e.g., Filter-DiskANN for filtered search [30], OOD-DiskANN for cross-modal search [31], and Fresh-DiskANN for streaming search [32]. Although DiskANN and its variants achieve a good performance on both memory overhead and search accuracy, they all ignore the fact that frequent SSD I/O would affect the overall QPS. This motivates us to address the I/O issue of DiskANN while retaining its strengths.

VIII. CONCLUSION

This paper proposes DiskANN++ that consists of three optimizations for DiskANN. (1) It expedites the convergence of graph search to the query neighborhood by employing query-sensitive entry vertex. (2) It applies isomorphic mapping on Vamana to refine its SSD layout and enhance each SSD page's data value. (3) It replaces original beamsearch by a new pagesearch based on the refined SSD layout with an asynchronous page expansion. Experimental results shows that DiskANN++ achieves a notable 1.5X to 2.2X improvement on QPS compared to DiskANN across various hardware configurations and datasets, given the same accuracy constraint.

ACKNOWLEDGMENT

This work was supported by the National NSF of China (62072149), the Primary R&D Plan of Zhejiang (2023C03198 and 2021C03156), and Fundamental Research Funds for the Provincial Universities of Zhejiang (GK219909299001-006).

REFERENCES

- [1] S. Arya and D. M. Mount, "Approximate nearest neighbor queries in fixed dimensions." in *SODA*, vol. 93, 1993, pp. 271–280.
- [2] P. Indyk and R. Motwani, "Approximate nearest neighbors: towards removing the eff curse of dimensionality," in *Proceedings of the thirtieth annual ACM symposium on Theory of computing*, 1998, pp. 604–613.
- [3] Q. Wang, H. Yin, T. Chen, J. Yu, A. Zhou, and X. Zhang, "Fast-adapting and privacy-preserving federated recommender system," *The VLDB Journal*, vol. 31, no. 5, pp. 877–896, 2022.
- [4] B. Sarwar, G. Karypis, J. Konstan, and J. Riedl, "Item-based collaborative filtering recommendation algorithms," in *Proceedings of the 10th international conference on World Wide Web*, 2001, pp. 285–295.
- [5] X. Xu, J. Liu, Y. Wang, and X. Ke, "Academic expert finding via (k, p) -core based embedding over heterogeneous graphs," in *2022 IEEE 38th International Conference on Data Engineering (ICDE)*. IEEE, 2022, pp. 338–351.
- [6] M. Flickner, H. Sawhney, W. Niblack, J. Ashley, Q. Huang, B. Dom, M. Gorkani, J. Hafner, D. Lee, D. Petkovic *et al.*, "Query by image and video content: The qbic system," *computer*, vol. 28, no. 9, pp. 23–32, 1995.
- [7] D. A. Adeniyi, Z. Wei, and Y. Yongquan, "Automated web usage data mining and recommendation system using k-nearest neighbor (knn) classification method," *Applied Computing and Informatics*, vol. 12, no. 1, pp. 90–108, 2016.
- [8] V. Bijalwan, V. Kumar, P. Kumari, and J. Pascual, "Knn based machine learning approach for text and document mining," *International Journal of Database Theory and Application*, vol. 7, no. 1, pp. 61–70, 2014.

- [9] T. Cover and P. Hart, "Nearest neighbor pattern classification," *IEEE transactions on information theory*, vol. 13, no. 1, pp. 21–27, 1967.
- [10] C. J. Zhu, T. Zhu, H. Li, J. Bi, and M. Song, "Accelerating large-scale molecular similarity search through exploiting high performance computing," in *2019 IEEE International Conference on Bioinformatics and Biomedicine (BIBM)*. IEEE, 2019, pp. 330–333.
- [11] M. Wang, X. Xu, Q. Yue, and Y. Wang, "A comprehensive survey and experimental comparison of graph-based approximate nearest neighbor search," *Proceedings of the VLDB Endowment*, vol. 14, pp. 1964–1978, 07 2021.
- [12] A. Gionis, P. Indyk, R. Motwani *et al.*, "Similarity search in high dimensions via hashing," in *Vldb*, vol. 99, no. 6, 1999, pp. 518–529.
- [13] L. Gong, H. Wang, M. Ogihara, and J. Xu, "idcc: indexable distance estimating codes for approximate nearest neighbor search," *Proceedings of the VLDB Endowment*, vol. 13, no. 9, 2020.
- [14] A. Arora, S. Sinha, P. Kumar, and A. Bhattacharya, "Hd-index: Pushing the scalability-accuracy boundary for approximate knn search in high-dimensional spaces," *Proceedings of the VLDB Endowment*, vol. 11, no. 8, 2018.
- [15] C. Silpa-Anan and R. Hartley, "Optimised kd-trees for fast image descriptor matching," in *2008 IEEE Conference on Computer Vision and Pattern Recognition*. IEEE, 2008, pp. 1–8.
- [16] H. Jegou, M. Douze, and C. Schmid, "Product quantization for nearest neighbor search," *IEEE transactions on pattern analysis and machine intelligence*, vol. 33, no. 1, pp. 117–128, 2010.
- [17] C.-Y. Chiu, A. Prayoonwong, and Y.-C. Liao, "Learning to index for nearest neighbor search," *IEEE transactions on pattern analysis and machine intelligence*, vol. 42, no. 8, pp. 1942–1956, 2019.
- [18] C. Fu, C. Xiang, C. Wang, and D. Cai, "Fast approximate nearest neighbor search with the navigating spreading-out graph," *arXiv preprint arXiv:1707.00143*, 2017.
- [19] Y. Malkov and D. Yashunin, "Efficient and robust approximate nearest neighbor search using hierarchical navigable small world graphs," *IEEE Transactions on Pattern Analysis and Machine Intelligence*, vol. PP, no. 4, pp. 824–836, 03 2016.
- [20] Q. Chen, B. Zhao, H. Wang, M. Li, C. Liu, Z. Li, M. Yang, and J. Wang, "Spann: Highly-efficient billion-scale approximate nearest neighborhood search," *Advances in Neural Information Processing Systems*, vol. 34, pp. 5199–5212, 2021.
- [21] M. Aumüller, E. Bernhardsson, and A. Faithfull, "Ann-benchmarks: A benchmarking tool for approximate nearest neighbor algorithms," *Information Systems*, vol. 87, p. 101374, 2020.
- [22] L. C. Shimomura, R. S. Oyamada, M. R. Vieira, and D. S. Kaster, "A survey on graph-based methods for similarity searches in metric spaces," *Information Systems*, vol. 95, p. 101507, 2021.
- [23] K. Aoyama, A. Ogawa, T. Hattori, T. Hori, and A. Nakamura, "Graph index based query-by-example search on a large speech data set," in *2013 IEEE International Conference on Acoustics, Speech and Signal Processing*. IEEE, 2013, pp. 8520–8524.
- [24] H. Hacid and T. Yoshida, "Neighborhood graphs for indexing and retrieving multi-dimensional data," *Journal of Intelligent Information Systems*, vol. 34, pp. 93–111, 2010.
- [25] R. Paredes and E. Chávez, "Using the k-nearest neighbor graph for proximity searching in metric spaces," in *String Processing and Information Retrieval: 12th International Conference, SPIRE 2005, Buenos Aires, Argentina, November 2-4, 2005. Proceedings 12*. Springer, 2005, pp. 127–138.
- [26] H. Simhadri, G. Williams, M. Aumüller, M. Douze, A. Babenko, D. Baranchuk, Q. Chen, L. Hosseini, R. Krishnaswamy, G. Srinivasa, S. Subramanya, and J. Wang, "Results of the neurips'21 challenge on billion-scale approximate nearest neighbor search," 05 2022.
- [27] S. Jayaram Subramanya, F. Devvrit, H. V. Simhadri, R. Krishnawamy, and R. Kadekodi, "Diskann: Fast accurate billion-point nearest neighbor search on a single node," *Advances in Neural Information Processing Systems*, vol. 32, 2019.
- [28] M. Dobson, Z. Shen, G. E. Blelloch, L. Dhulipala, Y. Gu, H. V. Simhadri, and Y. Sun, "Scaling graph-based anns algorithms to billion-size datasets: A comparative analysis," *arXiv preprint arXiv:2305.04359*, 2023.
- [29] J. Zhang, Z. Liu, W. Han, S. Xiao, R. Zheng, Y. Shao, H. Sun, H. Zhu, P. Srinivasan, W. Deng, Q. Zhang, and X. Xie, "Uni-retriever: Towards learning the unified embedding based retriever in bing sponsored search," in *KDD*, 2022, pp. 4493–4501.

- [30] S. Gollapudi, N. Karia, V. Sivashankar, R. Krishnaswamy, N. Begwani, S. Raz, Y. Lin, Y. Zhang, N. Mahapatro, P. Srinivasan, A. Singh, and H. V. Simhadri, "Filtered-diskann: Graph algorithms for approximate nearest neighbor search with filters," in *Proceedings of the ACM Web Conference 2023*, 2023, p. 3406–3416.
- [31] S. Jaiswal, R. Krishnaswamy, A. Garg, H. V. Simhadri, and S. Agrawal, "Ood-diskann: Efficient and scalable graph anns for out-of-distribution queries," *arXiv preprint arXiv:2211.12850*, 2022.
- [32] A. Singh, S. J. Subramanya, R. Krishnaswamy, and H. V. Simhadri, "Freshdiskann: A fast and accurate graph-based ann index for streaming similarity search," *arXiv preprint arXiv:2105.09613*, 2021.
- [33] X. Xu, M. Wang, Y. Wang, and D. Ma, "Two-stage routing with optimized guided search and greedy algorithm on proximity graph," *Knowledge-Based Systems*, vol. 229, p. 107305, 07 2021.
- [34] D. Dearholt, N. Gonzales, and G. Kurup, "Monotonic search networks for computer vision databases," vol. 2, 02 1988, pp. 548–553.
- [35] D. Zhu and M. Zhang, "Understanding and generalizing monotonic proximity graphs for approximate nearest neighbor search," *arXiv preprint arXiv:2107.13052*, 2021.
- [36] M. Babenko and A. Gusakov, "New exact and approximation algorithms for the star packing problem in undirected graphs," *Symposium on Theoretical Aspects of Computer Science (STACS2011)*, vol. 9, 03 2011.
- [37] K. Peng and Q. Huang, "Clustering approach based on mini batch kmeans for intrusion detection system over big data," *IEEE Access*, vol. PP, pp. 1–1, 02 2018.
- [38] M. Fiedler, "Algebraic connectivity of graphs," *Czechoslovak Mathematical Journal*, vol. 23, pp. 298–305, 1973. [Online]. Available: <https://api.semanticscholar.org/CorpusID:117770486>
- [39] C. Zhang, F. Wei, Q. Liu, Z. Tang, and Z. Li, "Graph edge partitioning via neighborhood heuristic," 08 2017, pp. 605–614.
- [40] C. Xie, L. Yan, W.-J. Li, and Z. Zhang, "Distributed power-law graph computing: Theoretical and empirical analysis," *Advances in Neural Information Processing Systems*, vol. 2, pp. 1673–1681, 01 2014.
- [41] F. Petroni, L. Querzoni, K. Daudjee, S. Kamali, and G. Iacoboni, "Hdrrf: Stream-based partitioning for power-law graphs," 10 2015, pp. 243–252.
- [42] G. Karypis, V. Kumar, and S. Comput, "A fast and high quality multilevel scheme for partitioning irregular graphs," *SIAM Journal on Scientific Computing*, vol. 20, 02 1970.
- [43] I. Stanton and G. Kliot, "Streaming graph partitioning for large distributed graphs," 09 2012.
- [44] C. Tsourakakis, C. Gkantsidis, B. Radunovic, and M. Vojnovic, "Fennel: Streaming graph partitioning for massive scale graphs," 02 2014, pp. 333–342.
- [45] H. Wei, J. Yu, C. Lu, and X. Lin, "Speedup graph processing by graph ordering," 06 2016, pp. 1813–1828.
- [46] E. Facco, M. d'Errico, A. Rodriguez, and A. Laio, "Estimating the intrinsic dimension of datasets by a minimal neighborhood information," *Scientific Reports*, vol. 7, 09 2017.
- [47] Anon. (2010) Datasets for approximate nearest neighbor search. [Online]. Available: <http://corpus-texmex.irisa.fr/>
- [48] A. Yandex and V. Lempitsky, "Efficient indexing of billion-scale datasets of deep descriptors," 06 2016, pp. 2055–2063.
- [49] Song. (2011) Million song dataset benchmarks. [Online]. Available: <http://www.ifs.tuwien.ac.at/mir/msd/>
- [50] Crawl. (2023) Common crawl. [Online]. Available: <http://commoncrawl.org/>
- [51] H. Zhang, X. Song, C. Xiong, C. Rosset, P. Bennett, N. Craswell, and S. Tiwary, "Generic intent representation in web search," 07 2019, pp. 65–74.
- [52] P. Jeffrey, S. Richard, and D. M. Christopher. (2015) Glove: Global vectors for word representation. [Online]. Available: <http://nlp.stanford.edu/projects/glove/>
- [53] microsoft, "Sptag: A library for fast approximate nearest neighbor search," <https://github.com/microsoft/SPTAG>, 2023.
- [54] Zilliztech, "Bbann: Block-based approximate nearest neighbor," <https://github.com/zilliztech/BBAnn>, 2023.
- [55] microsoft, "Diskann," <https://github.com/microsoft/DiskANN>, 2023.
- [56] W. Li, Y. Zhang, Y. Sun, W. Wang, M. Li, W. Zhang, and X. Lin, "Approximate nearest neighbor search on high dimensional data—experiments, analyses, and improvement," *IEEE Transactions on Knowledge and Data Engineering*, vol. 32, no. 8, pp. 1475–1488, 2019.
- [57] H. Jégou, M. Douze, and C. Schmid, "Product quantization for nearest neighbor search," *IEEE transactions on pattern analysis and machine intelligence*, vol. 33, pp. 117–28, 01 2011.
- [58] T. Ge, K. He, Q. Ke, and J. Sun, "Optimized product quantization for approximate nearest neighbor search," in *Proceedings of the IEEE Conference on Computer Vision and Pattern Recognition*, 2013, pp. 2946–2953.
- [59] Y. Kalantidis and Y. Avrithis, "Locally optimized product quantization for approximate nearest neighbor search," in *CVPR*, pp. 2321–2328, 01 2014.
- [60] J. Wang and T. Zhang, "Composite quantization," *IEEE Transactions on Pattern Analysis and Machine Intelligence*, vol. PP, 12 2017.
- [61] Z. Pan, L. Wang, Y. Wang, and Y. Liu, "Product quantization with dual codebooks for approximate nearest neighbor search," *Neurocomputing*, vol. 401, 03 2020.
- [62] Y. Weiss, A. Torralba, and R. Fergus, "Spectral hashing," in *Advances in Neural Information Processing Systems*, D. Koller, D. Schuurmans, Y. Bengio, and L. Bottou, Eds., vol. 21. Curran Associates, Inc., 2008.
- [63] H. Xu, J. Wang, Z. Li, G. Zeng, S. Li, and N. Yu, "Complementary hashing for approximate nearest neighbor search," 11 2011, pp. 1631–1638.
- [64] Q. Huang, J. Feng, Q. Fang, W. Ng, and W. Wang, "Query-aware locality-sensitive hashing scheme for lp norm," *The VLDB Journal*, vol. 26, no. 5, pp. 683–708, 2017.
- [65] S. Karaman, X. Lin, X. Hu, and S.-F. Chang, "Unsupervised rank-preserving hashing for large-scale image retrieval," in *Proceedings of the 2019 International Conference on Multimedia Retrieval*, 2019, pp. 192–196.
- [66] K. Hajebi, Y. Abbasi-Yadkori, H. Shahbazi, and H. Zhang, "Fast approximate nearest-neighbor search with k-nearest neighbor graph," in *Twenty-Second International Joint Conference on Artificial Intelligence*, 2011.
- [67] Y. Malkov, A. Ponomarenko, A. Logvinov, and V. Krylov, "Approximate nearest neighbor algorithm based on navigable small world graphs," *Information Systems*, vol. 45, pp. 61–68, 2014.
- [68] C. Fu and D. Cai, "Efanna : An extremely fast approximate nearest neighbor search algorithm based on knn graph," 09 2016.
- [69] M. Zhang and Y. He, "Grip: Multi-store capacity-optimized high-performance nearest neighbor search for vector search engine," in *Proceedings of the 28th ACM International Conference on Information and Knowledge Management*, 11 2019, pp. 1673–1682.
- [70] J. Ren, M. Zhang, and D. Li, "Hm-ann: Efficient billion-point nearest neighbor search on heterogeneous memory," *Advances in Neural Information Processing Systems*, vol. 33, pp. 10 672–10 684, 2020.